AD-A092 479 AIR FORCE INST OF TECH WRIGHT-PATTERSON AFB OH F/G 4/2
A NEW HORIZONTAL GRADIENT, CONTINUOUS FLOW, ICE THERMAL DIFFUSI--ETC(U)
JUN 80 E M TOMLINSON
UNCLASSIFIED AFIT-CI-80-210 NL

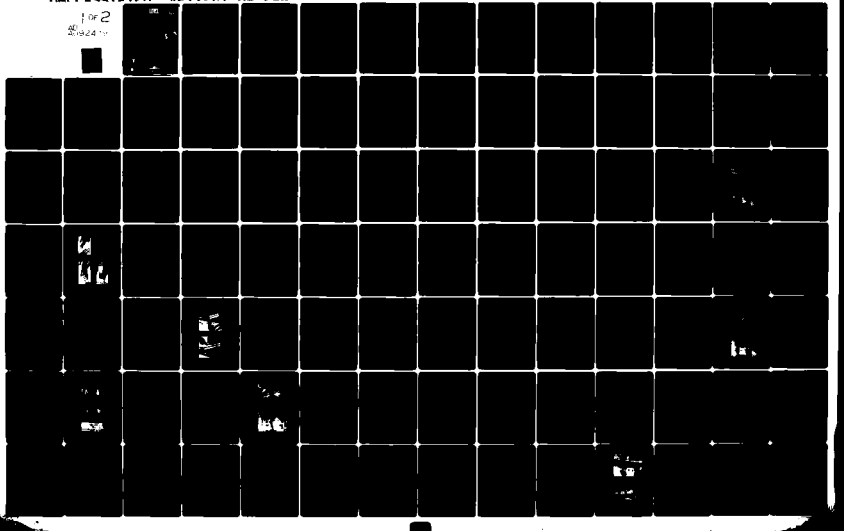

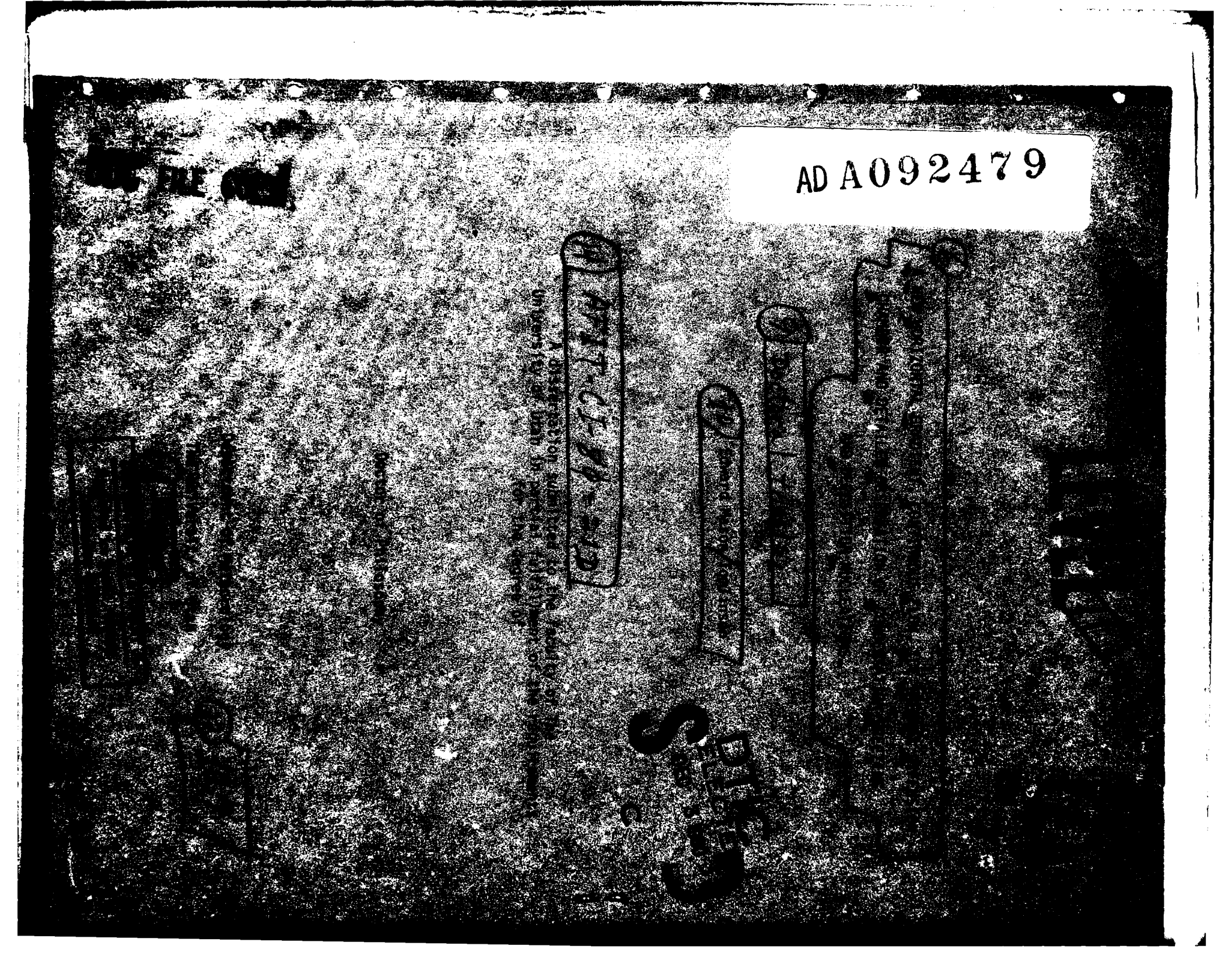

80-21

AFIT RESEARCH ASSESSMENT

The purpose of this questionnaire is to ascertain the value and/or contribution of research accomplished by students or faculty of the Air Force Institute of Technology (ATC). It would be greatly appreciated if you would complete the following questionnaire and return it to:

AFIT/NR
Wright-Patterson AFB OH 45433

Research Title: A New Horizontal Gradient, Continuous Flow, Ice Thermal Diffusion Chamber and Detailed Observation of Condensation-Freezing and Deposition Nucleations

Author: Edward Mason Tomlinson

Research Assessment Questions:

1. Did this research contribute to a current Air Force project?

   a. Yes b. No

2. Do you believe this research topic is significant enough that it would have been researched (or contracted) by your organization or another agency if AFIT had not?

   a. Yes b. No

3. The benefits of AFIT research can often be expressed by the equivalent value that your agency achieved/received by virtue of AFIT performing the research. Can you estimate what this research would have cost if it had been accomplished under contract or if it had been done in-house in terms of manpower and/or dollars?

   a. Man-years _____. b. $_____

4. Often it is not possible to attach equivalent dollar values to research, although the results of the research may, in fact, be important. Whether or not you were able to establish an equivalent value for this research (3 above), what is your estimate of its significance?

   a. Highly Significant b. Significant c. Slightly Significant d. Of No Significance

5. AFIT welcomes any further comments you may have on the above questions, or any additional details concerning the current application, future potential, or other value of this research. Please use the back of this questionnaire for your statement(s).

NAME GRADE POSITION

ORGANIZATION LOCATION

A NEW HORIZONTAL GRADIENT, CONTINUOUS FLOW, ICE THERMAL DIFFUSION CHAMBER AND DETAILED OBSERVATION OF CONDENSATION-FREEZING AND DEPOSITION NUCLEATIONS

by

Edward Mason Tomlinson

A dissertation submitted to the faculty of The University of Utah in partial fulfillment of the requirements for the degree of

Doctor of Philosophy

Department of Meteorology

The University of Utah

June 1980

THE UNIVERSITY OF UTAH GRADUATE SCHOOL

SUPERVISORY COMMITTEE APPROVAL

of a dissertation submitted by

Edward M. Tomlinson

I have read this dissertation and have found it to be of satisfactory quality for a doctoral degree.

2 May 1980 — Norihiko Fukuta
Date — Norihiko Fukuta
Chairman, Supervisory Committee

I have read this dissertation and have found it to be of satisfactory quality for a doctoral degree.

May 2, 1980 — S. K. Kao
Date — S. K. Kao
Member, Supervisory Committee

I have read this dissertation and have found it to be of satisfactory quality for a doctoral degree.

May 2, 1980 — Julia N. Paegle
Date — Julia N. Paegle
Member, Supervisory Committee

I have read this dissertation and have found it to be of satisfactory quality for a doctoral degree.

May 2, 1980 — Kenneth Sassen
Date — Kenneth Sassen
Member, Supervisory Committee

I have read this dissertation and have found it to be of satisfactory quality for a doctoral degree.

May 2, 1980 — Robert E. Stephenson
Date — Robert E. Stephenson
Member, Supervisory Committee

THE UNIVERSITY OF UTAH GRADUATE SCHOOL

FINAL READING APPROVAL

To the Graduate Council of The University of Utah:

I have read the dissertation of Edward M. Tomlinson in its final form and have found that (1) its format, citations, and bibliographic style are consistent and acceptable; (2) its illustrative materials including figures, tables, and charts are in place; and (3) the final manuscript is satisfactory to the Supervisory Committee and is ready for submission to the Graduate School.

May 13, 1980
Date

Norihiko Fukuta
Norihiko Fukuta
Member, Supervisory Committee

Approved for the Major Department

S. K. Kao
S. K. Kao
Chairman, Dean

Approved for the Graduate Council

James L. Clayton
Dean of The Graduate School

05
6-76

ABSTRACT

It is well recognized that conditions in the environment surrounding ice nucleu (IN) particles must be accurately controlled in order to understand their nucleation behavior. Concerning the condensation-freezing and deposition mechanisms of ice nucleation, the main factors representing the environment are supersaturation and supercooling (temperature). Starting from the concept of the wedge-shaped ice thermal diffusion chamber of Schaller and Fukuta, and that of the Fukuta-Saxena cloud condensation nucleus (CCN) spectrometer, and by additionally considering operational efficiency and accuracy, a continuous-flow, horizontal gradient, ice thermal diffusion chamber has been developed. The chamber consists of three parts, i.e., preprocessing, main activation and ice crystal settling sections. A common top plate is used for all three sections and is held isothermal using a circulating bath while a temperature gradient is maintained across the bottom plate of the main section by applying thermoelectric modules. In the preprocessing and main sections, both plates are covered with ice. A newly developed method is applied to smoothly coat ice on the plates. This configuration of the main section results in a nearly constant temperature horizontally in the direction across the sample flow, and produces a range of supersaturations. Heat pipes are utilized on the sides of the bottom plate to insure temperature uniformity along the direction of the flow. The sample volume is sandwiched in the region of maximum supersaturation between layers of filtered and predried air such that,

as the sample enters the main section, a nearly constant supersaturation is achieved vertically through the sample without transient supersaturations. The preprocessing section is held isothermal at the top plate temperature. The design and flow of the main section permit the nucleated ice crystals to be carried into the ice crystal settling section without loss. The bottom plate in the settling section is maintained at a temperature slightly lower than that of the top plate. Formation of transient supersaturations at the entrance of the settling section has been avoided by delaying vapor diffusion while allowing thermal diffusion to proceed. The problem of transient supersaturation development has been examined for shear (Poiseuille) flow cases using a numerical method instead of the commonly used slab flow assumption. Wall effects have also been computed for the supersaturation distribution. The stability of the sample flow throughout the entire chamber has been confirmed with smoke tests. A new method for ice crystal detection has been developed and is employed in the ice crystal settling section. Mylar copy film (carbon paper) holding condensed water droplets is placed in the settling section. Ice crystals nucleated in the main section fall on the film and grow to visible sizes in the presence of the droplets. The positions of the ice crystals across the flow direction give the supersaturations and temperatures at which they nucleated. The optimum design of the chamber in terms of the height, width, length and flow speed has been determined.

Two numerical models have been developed to compute the temperature and supersaturation fields within the chamber. The first computes the steady state conditions in a vertical plane perpendicular to the flow

and includes the wall effects. The second computes the steady state conditions in a vertical plane parallel to the flow using the shear flow velocity profile and the total pressure- and temperature-dependent coefficients for vapor and thermal diffusion.

The increased accuracy of the developed chamber has resulted in several significant new findings. For all the temperature and supersaturation ranges studied, the rate of deposition nucleation is much lower than that for condensation-freezing. For silver iodide (AgI) particles of average diameter 0.05 μm, only a small fraction are active below 1% water supersaturation, while for 1,5 - dihydroxynaphthalene (DN) of average diameter 0.1 μm, a much larger fraction are active. The total number of active nuclei for these samples was approximately three times greater for DN than for AgI at high supersaturations. For temperatures warmer than -10°C, the condensation-freezing mechanism is not effective for AgI. Natural nuclei and kaolinite show little supersaturation dependence below 1% water supersaturation and as much as an order of magnitude increase as water supersaturation increases from 1% to 2.5%. Additionally for natural nuclei, large variances were observed with high counts in cloud downdrafts and low counts during precipitation.

TABLE OF CONTENTS

TABLE OF CONTENTS (Continued)

LIST OF FIGURES

LIST OF FIGURES (Continued)

LIST OF FIGURES (Continued)

ACKNOWLEDGMENTS

I wish to express my appreciation to the entire faculty, staff, and graduate students of the Meteorology Department. Their interest and concern helped me through many difficult times. In particular, Dr. Fukuta offered guidance and support throughout the research. His assistance aided in finding many solutions to both large and small problems. The technical advice of Dr. Sassen and Dr. Saxena was very helpful. The remaining members of my committee were of great assistance with their comments and suggestions. A very special thank you to Mrs. Deanna Plumhof, my typist, for her congenial cooperation and very special efforts. Dr. Jan Paegle's expertise was greatly appreciated during the numerical modeling phases and both his and Dr. Julia Paegle's encouragement was always greatly appreciated.

I would like to thank Rich Coleman for the many times he helped with my diverse problems, especially with the computer. Byron Minchow aided me greatly in the data collection phase of my research. Hector Vasques and Abe Santos deserve a large thank you for all of their help and support.

And to my family, Harriet, Susan and David, my sincere thanks for doing without a full time husband and father. I love you all very much. And especially to my wife, thanks for waiting.

The Air Force Office for Scientific Research contributed funds for equipment support, without which this research would not have been possible. I am very grateful for this support.

CHAPTER 1

INTRODUCTION

The occurrance of precipitation in the atmosphere has a large impact on man's activities, often dictating where civilizations locate, how they evolve and even whether they survive. The absence of precipitation brings famine and despair whereas an over-abundance can also lead to similiar results. Mankind has to a large extent adapted to the global distribution of precipitation by migrating to regions where precipitation is adequate and avoiding those where moisture supplies are inadequate. However, even within regions of normally adequate precipitation, short or long term fluctuations can result in drought or flooding and thereby exert significant effects on man's environment. Both the geographic and time variances are to a large extent a result of fluctuating moisture availability in the environment. However, the mechanisms involved in the process of converting the water suspending in the atmosphere into precipitation elements also play significant roles. Hence, the study of these mechanisms involved in precipitation formation is of great importance to man.

Precipitation transports moisture from the atmosphere to the earth's surface in various forms including rain, snow, hail and graupel (Petersen, 1958). It is important to note that with the exception of some tropical showers, the ice phase is always involved in the precipitation formation process even when the final form observed on the ground is rain (Mason, 1971). These raindrops form when ice crystals

grow in supercooled clouds (i.e. clouds consisting of water droplets below 0°C) and subsequently fall and melt at lower altitudes. This mechanism of precipitation formation, known as the Bergeron mechanism, plays a dominant role in the atmosphere (Bergeron, 1935). It is the process of the initial ice crystal formation involved in this mechanism that receives primary attention in this study.

Formation of ice crystals or ice nucleation must take place at least at the early stage and possibly throughout the Bergeron process of precipitation formation. Ice crystal nucleation can be categorized into two types, i.e. homogeneous and heterogeneous. In the former, the phase change to the solid (crystal) state occurs without the assistance of a foreign substance while the latter involves some foreign particle or substrate in the phase change process. Such particles are called *ice nuclei*. Since temperatures of -40°C or lower are required for homogeneous ice nucleation (Shaefer, 1948), the occurrence of significant numbers of natural ice crystals in atmospheric processes at much warmer temperatures indicates that this is not the primary mechanism in nature in most cases and in fact formation of the cirrus anvils associated with thunder or hail clouds is probably one of the rare examples of the process in the atmosphere. This leaves heterogeneous nucleation as the contributing mechanism for ice crystal formation for most cases in nature (Weickmann, 1971; Rodgers, 1976).

Investigators studying heterogeneous ice nucleation in the atmosphere have determined that there are large fluctuations, both in time and space, in the number of particles which act as ice nuclei and furthermore that their number is normally quite small compared to the number of cloud condensation nuclei (i.e. nuclei which aid the formation

of cloud droplets)(Fukuta, 1966; Weickmann, 1971). Three orders of magnitude differences are quite common between the ice and the cloud condensation nuclei. This scarcity of natural ice nuclei leads investigators to the realization that opportunities may exist to enhance the precipitation process by artificially adding effective ice nuclei to a supercooled cloud environment. Therefore, the study of ice nucleation in the atmosphere concentrates on the effective number and activation characteristics of heterogeneous ice nuclei both naturally occurring and artificially generated. For ice nuclei existing naturally in the atmosphere, the studies have had very limited success due mainly to the scarcity and variability of these particles. Cloud physicists have found materials which, when dispersed properly into a supercooled cloud environment, behave as effective heterogeneous ice nuclei. These include silver iodide, lead iodide, metaldehyde and 1,5-dihydroxynaphthalene. These ice nuclei have been studied extensively but findings have been inconsistent due primarily to the differences in the methods of measurement reflected in the designs of instrumentation used (Hallett, 1971; Schaefer, 1971; Langer, 1973; Vali, 1976).

The previous studies have indicated that there are three distinct mechanisms for heterogeneous ice nucleation (Schaller and Fukuta, 1979). The first, deposition nucleation involves the direct transition from the vapor to the solid state with some foreign particles acting as the nuclei for crystallization. The condensation-freezing nucleation mechanism involves all three states, with vapor condensing around the nucleus to form a liquid droplet which supsequently freezes. The final mechanism, contact-freezing nucleation, also produces a crystal in the supercooled droplet but the nucleus is external to the droplet and

initiates freezing upon contact with the droplet surface. Each mechanism has its own dependencies on temperature, supersaturation, and time as well as on the characteristics of the nuclei involved.

Researchers have used many different methods in their study of ice nuclei but generally they can be grouped into three categories, the cloud chamber method, the filter method and the large crystal method. Most mixing chambers sustain supercooled clouds in them as a reproduction of atmospheric conditions and permit studying the behavior of ice nuclei injected in the clouds. There are a few problems associated with this method. First, during the processes of sample ice nuclei introduction and humidification, transient supersaturation is likely to occur, making the condition of ice nuclei activation unclear. Second, only one supersaturation level, i.e. water saturation, can be stably sustained. Third, ice nuclei behaviors under different levels of supersaturation cannot be studied. Different levels of supersaturations can be produced by expansion chambers but they cannot be sustained under steady state. In addition, ice crystal counts obtained are results of different ice nucleation mechanisms occurring simultaneously.

The filter method allows the ice nuclei removed from the air to be activated under different supersaturations and temperatures. Results obtained by this method, however, suffer from effects of coexisting impurities and substrate.

While the clean faces of large cleaved single crystals of an ice nucleus compound furnish excellent macroscopic surfaces for studying ice nucleation mechanisms, the important size effect of the nuclei is lost in addition to unrealistically magnified effect of steps and cavities (Schaller and Fukuta, 1979).

Although these methods have different advantages and disadvantages in heterogeneous ice nucleation studies, the cloud chamber method can avoid the substrate problem and does include the size effect. Therefore, use of a cloud chamber would give the best opportunity to gather reliable and consistent data, had the difficulty of changing and maintaining the supersaturation at different levels been solved.

Thermal diffusion cloud chambers are capable of stably maintaining temperature and supersaturation at any combined levels, thereby eliminating the above mentioned deficiency of cloud chambers. The existing cloud chambers of this type, however, can only accommodate small sample volumes, hold one set of temperature and supersaturation at the desired portion of the chambers, and the counting schemes employed are unreliable (normally visual method). The wedge-shaped ice thermal diffusion chamber recently introduced by Schaller and Fukuta (1979) produces a range of supersaturation and therefore eases the disadvantage of single set of temperature and supersaturation in the normal thermal diffusion cloud chambers. However, it still suffers from the small sampling volume. In addition, the time dependency of ice nucleation cannot be accurately studied. The purpose of this study is to design and construct a new horizontal gradient, continuous flow, ice thermal diffusion cloud chamber which maintains the assets of the present chambers while eliminating some of the difficulties. This new cloud chamber is then used to study various ice nuclei and identify their nucleation mechanisms as well as their dependence on temperature and supersaturation.

A review of the previous methods of ice nuclei study is presented in Chapter 2. Chapter 3 includes the design and construction of the

new chamber with a discussion of the distinct improvements over previous chambers. The numerical models used to simulate the conditions in the chamber are included in Chapter 4. Chapter 5 presents the procedure of chamber operation and sampling. Results and discussions are included in Chapter 6 with conclusions in Chapter 7.

CHAPTER 2

METHODS USED IN PREVIOUS ICE NUCLEATION STUDIES

Since the primary purpose for studying ice nuclei is to understand their behaviors under naturally existing conditions, it is highly desirable to reproduce the conditions as faithfully as possible (Podzimek, 1971). For studies performed under unnatural conditions, the results must be manipulated to compensate for these deviations. Any instrument which can accurately control the environment within the restraints of nature will therefore have a significant advantage over instruments where unnatural conditions exist, even if only for short periods of time.

For ice nucleation studies, temperature has always been an important parameter and has been fairly accurately controlled in most studies (Mason and Hallett, 1956; Bigg, 1957). The more recent recognition of the roles of supersaturation in heterogeneous ice nucleation has clarified the importance of its accurate, though difficult, control (Hudson and Squires, 1976; Schaller and Fukuta, 1979). The techniques used in ice nucleation studies are surveyed below and should be critically evaluated for their control of temperature and supersaturation in order to determine the usefulness of the results when applied to realistic atmospheric conditions.

2.1 Cloud Chambers

Although there are a variety of types of cloud chambers, their basic

purpose is to furnish an enviroment of a supercooled cloud in which ice nucleation can be studied. Schaefer (1946) first used a small commercial freezer as a cloud chamber by blowing breath into it, and since then other investigators have developed various types of cold chambers, each with its own distinct advantages and/or disadvantages.

2.1.1 Mixing chambers

The walls of mixing chambers are normally maintained at a constant temperature with the supercooled cloud formed either by cooling the sample air below its dew point temperature or by the addition of water vapor or droplets. The intent is to provide an isothermal environment with a constant supersaturation field; but in reality, cloud temperatures can vary up to 5°C (Bigg, 1957) and large fluctuations in supersaturation often occur (Ohtake, 1976). In addition, selection of steady state supersaturation at an arbitrary level is not possible, and the values which do occur cannot be accurately determined. There also exists the possibility of transient supersaturations (i.e. supersaturations of short duration which are much greater than the final values). These tend to result in unrealistically high numbers of active nuclei.

2.1.2 Expansion chambers

Expansion chambers were originally used in nuclear physics to trace cosmic rays (Sears and Zemansky, 1962) and later adapted for use in cloud physics. For ice nucleation studies, the air is normally cooled to a subfreezing temperature and then further cooled by rapid adiabatic expansion (Warner, 1957). The results are reasonably reproduciable for a given instrument, but a significant variance has been

noted between different chambers, even ones with identical design (Kline and Brier, 1961). Expansion chambers are reliable and readily adaptable for both field and laboratory use but suffer from some basic disadvantages. The expansion produces short term supercooling and supersaturation, which can be estimated with reasonable accuracy, but the effect of the short-lived conditions cannot be exactly evaluated. Normally, the transient supersaturations produced in the chamber are much higher than those which occur in nature, resulting in unreliably high nuclei counts.

2.1.3 Diffusion chambers

Langsdorf developed a diffusion cloud chamber for use in nuclear physics in 1936. He suggested that it might be useful for atmospheric studies, but it was not utilized for such work until Schaefer developed several types for atmospheric use (Schaefer, 1952, 1954). These chambers are convectively stable and are capable of reproducing temperatures and supersaturation fields with excellent accuracy (Squires, 1972). Caution must be taken to avoid wall effects and transient supersaturations while ensuring that the counting method employed yields accurate results. On the other hand, thermal diffusion chambers suffer from the disadvantage of necessarily having small heights and consequently small volumes (Squires, 1971), thereby limiting their use for samples with a small ice nuclei population (Hallett, 1971).

2.2 Precipitation Methods

Instruments using this method collect the ice nuclei on substrates and subsequently activate them under controlled temperatures and

supersaturations and then grow the crystals to detectable size. Although these methods yield information about the sizes of the nuclei, they are critically dependent on the development procedure and suffer from a lack of reproducibility (Langer, 1973). Furthermore, the effect of the substrate can contribute significantly to the apparent activation characteristics of the nuclei.

2.2.1 Impaction method

Ice nuclei particles are allowed to impact on some surface and are subsequently developed. Impaction on a varnished surface was used by Yang (1962) while Gerber (1976) used a foil in the Goetz aerosol spectrometer. The collection efficiency of these methods is somewhat uncertain and the substrate problem is certainly present.

2.2.2 Membrance filter method

This method makes possible the sampling of large volumes of air with a relatively simple experimental setup. The method of using millipore filters was first employed by Bigg, et al., (1961) and has subsequently been used by many investigators (Bigg, et al., 1963). The method, however, is dependent on the type of filter used, the amount of air drawn through it, and the development process. Again, significant substrate effect is expected with this method.

2.3 Use of Thermal Diffusion Chambers for Cloud Condensation Nuclei (CCN) Studies

Of all the types of instruments used in atmospheric nuclei studies, the thermal diffusion chamber is unique in its ability to produce accurately controlled temperature and supersaturation fields under steady state while avoiding the troublesome substrate effects and incoporating

the size effect. These chambers operate with a thermally stable interior environment where the temperature profiles can be precisely determined. As is the case in all other ice nucleus detection methods, the supersaturation values cannot be directly measured. However, with known boundary conditions for vapor pressure and temperature, the supersaturation fields can be accurately computed. Adequate knowledge of these parameters permits detailed studies of ice nuclei to be performed.

The thermal diffusion chambers used in atmospheric studies have taken many different designs. Concentric cylinders with wetted wall have been used (Rosen and Hofmann, 1977) although the most common design utilizes parallel plates (Katz and Ostermier, 1967; Radke and Hobbs, 1969; Elliott, 1971; Heist and Reiss, 1973). While most of the thermal diffusion chambers process the sample under static conditions, in recent years, continuous flow thermal diffusion chambers have been developed. Table 1 lists the use of thermal diffusion chambers in the study of atmospheric CCN (Schaller, 1975).

2.4 Use of Thermal Diffusion Chambers for Ice Nuclei (IN) Studies

By lowering the temperature and substituting ice surfaces for the wetted ones, the thermal diffusion chambers used for CCN studies can in principle be applied to ice nuclei studies. Diffusion chambers were used in IN studies to develope filters as discussed earlier in addition to investigating ice nucleation both on large crystal surfaces and on particles freely suspended in air.

2.4.1 For studies using large crystal surfaces

By placing a crystal surface in the interior of a thermal diffusion chamber, the environment over the surface can be controlled

TABLE 1. THERMAL DIFFUSION CHAMBERS

Year	Investigators	Operating Supersaturations, %	Counting Technique	Aerosols Investigated
1953	Schiff et al.	1 to 15	Not used	NaCl, $CaCl_2$, $CuSO_4$, AgI, $MnCl_4$, LiCl; measurements of critical supersaturation reported.
1956	Wieland	0.1 to 1	Droplet impressions on varnish layer	NaCl nuclei from seawater; natural aerosol in the ground layer at Locarno-Monti, Italy.
1961	Storozhilova	0 to 12	Microscope	Atmospheric aerosol (USSR); room aerosol; AgI, NaCl
1963	Twomey	0.1 to 3	Direct photography	Natural aerosol in North America and Australia.
1964	Severynse	0.1 to 4	Droplet impressions on a carbon-coated glass disk	Natural aerosol at Montauk Point, Long Island, N. Y., eastern coast of the U. S.
1967	Laktionov	0.1 to 4	Photoelectric counter	Natural aerosol near Obnisk, USSR
1968	Kocmond and Jiusto	0.1 to 3	Direct photography	Natural aerosol near Buffalo, N. Y.
1968	Gagin and Terliuc	0.02 to 1	Direct photography	Results not reported.
1969	Radke and Hobbs	0.2 to 1	Laser beam scattering	Natural aerosol in the Olympic Mts. of Washington State, aerosol produced by forest fire near Eatonville, Wash.

TABLE 1 (Continued)

Year	Investigators	Operating Supersaturations, %	Counting Technique	Aerosols Investigated
1969	Ohta and Uchida		Measurement of the transmitted beam intensity	Results not available.
1970	Saxena et al.	0.2	Direct photography	Natural aerosol in Rolla Mo.
1972	Auer	0.5 to 3.5	Direct photography	St. Louis, Mo. natural aerosol
1973	Fitzgerald and Spyers-Duran	0.17 to 1	Direct photography	St. Louis, Mo. natural aerosol
1974	Saxena and Fukuta	0.1 to	Climet Particle Analyzer	Denver, Co. natural aerosol
1976	Hudson and Squires	0.1 to 1	Royco counter	Reno, Nevada natural aerosol

precisely and ice nucleation can be studied in detail. Unfortunately, the results of these studies cannot be applied directly to atmospheric processes since the size effect is not incorporated (Fletcher, 1958) and the effect of the large substrate is not known.

2.4.2 For studies of freely suspended nuclei

The attributes of the thermal diffusion chamber method have been utilized very effectively by Schaller and Fukuta (1979) in a wedge-shaped chamber. The isothermal plates were replaced with ones where a temperature gradient is maintained across the plates, thereby producing a center environment where a range of supersaturations exist. This chamber allowed the detailed study of artificial ice-nucleating agents, but the limited volume precluded its use for natural aerosols. The visual counting method leaves some room for error, and wall effects may affect the interior environment.

2.5 Principle of Operation of Thermal Diffusion Chamber

Since the thermal diffusion chamber method is capable of the accurate temperature and supersaturation control while avoiding substrate effects and including size effects, it has the best promise for use in detailed ice nuclei studies. The mechanism whereby ice and water supersaturations are sustained in subfreezing temperature ranges is illustrated in Figure 1. The thermal diffusion chamber works by evaporating water vapor from a saturated warm surface (the top plate), diffusing it through the chamber interior and condensing it on a cooled surface (the bottom plate). The top plate is ice covered and maintained at a temperature T_t. The bottom plate is also ice covered and maintained at another temperature T_b where $T_b<T_t$. Katz and Mirabel (1975) showed

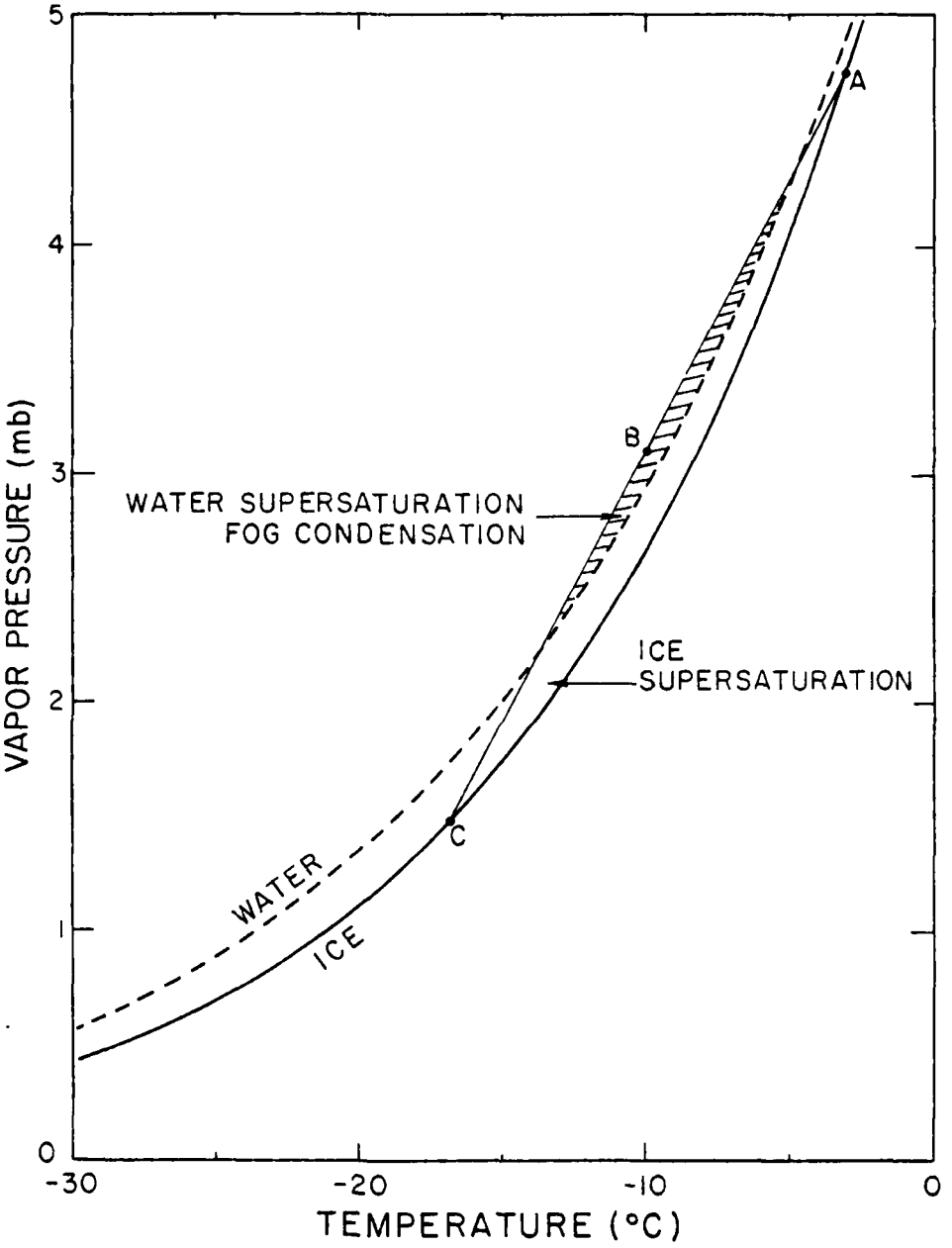

Figure 1. Principle of supersaturation development in thermal diffusion chambers. Point A is at the top plate temperature, C at the bottom plate temperature, with point B representing the conditions at the midpoint between the plates.

that the temperature and vapor pressure profiles between the plates are very close to linear. This profile is shown in Figure 1 by the straight line from A to C. However, the saturation values for both ice and water form curves which are concave upward with the curve for water saturation slightly above that for ice. Hence, for ice coated boundaries where the temperature is known, the vapor pressure can be accurately determined using the ice saturation values. In Figure 1, the top and bottom plate values are given by points A and C, respectively. The linear profile through the interior results in vapor pressure, P, higher than ice saturation, P_{si}, and ice supersaturation results. Ice supersaturation is defined as $S_i = (P/P_{si})-1$. For sufficiently large temperature differences, vapor pressure values greater than water saturation, P_{sw}, exist and water supersaturated conditions are created. Water supersaturation is defined as $S_w = (P/P_{sw})-1$. These temperature and vapor pressure profiles produce maxima for both water and ice supersaturation around the chamber center, but they are not necessarily colocated.

Most thermal diffusion chambers in use have isothermal plates which produce the same temperature and vapor pressure profiles throughout the chamber interior except for the regions close to the walls. The chamber center is maintained at a constant temperature and supersaturation. The CCN spectrometer of Fukuta and Saxena (1979a) as well as the wedge-shaped ice thermal diffusion chamber of Schaller and Fukuta (1979) incorporate temperature gradients on the plates, thereby creating a range of supersaturations horizontally across the chamber center. This allows a sample to be studied under a range of supersaturations during an experimental run instead of under only a single value of supersaturation. This not only expedites the sampling procedure but minimizes

the errors caused by changes in the sample between experiments.

The ice thermal diffusion chamber presented in this study is somewhat different from the two mentioned above in that the top plate is held isothermal while a temperature gradient is maintained across the bottom plate. The result is again a range of supersaturation across the chamber center with an accompanying small temperature change. Figure 2 illustrates a typical case where the two lines ABC and ADE in part (a) show the extremes which occur in the sample. The positioning of the sample will be explained in the next chapter. It should be noted in Figure 2(b) that water supersaturation exists only in a portion of the chamber while ice supersaturation exists throughout the interior.

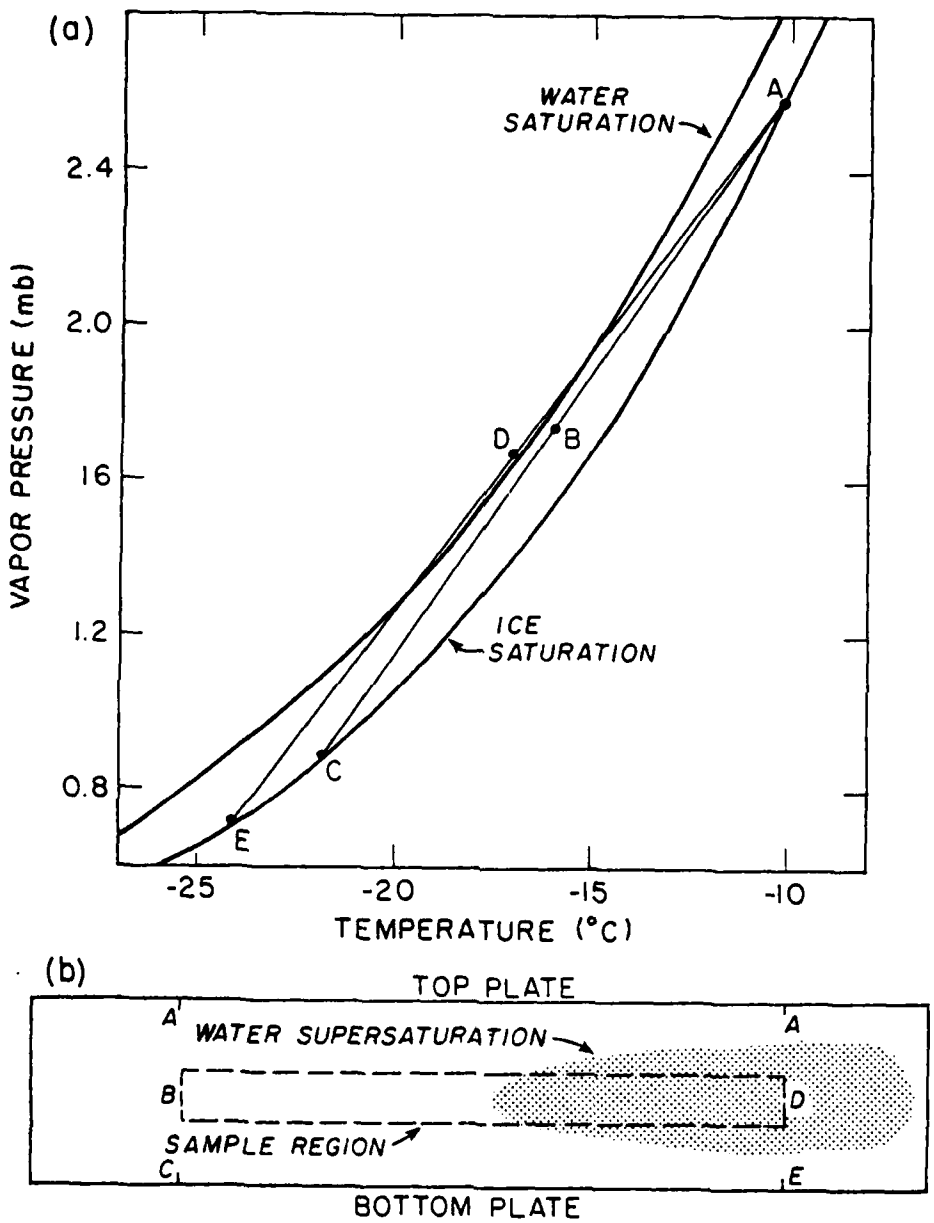

Figure 2. The method used in the present study which creates a range of supersaturations in the chamber.

CHAPTER 3

APPARATUS

3.1 Factors to be Considered in the Design

Any instrument used for the detailed study of ice nuclei behavior must be capable of accurately controlling both the temperature and the supersaturation of the environment in which the nuclei are activated since ice nucleation is normally a function of both variables (Schaller and Fukuta, 1979). As discussed earlier, thermal diffusion chambers allow accurate control of these variables if the boundaries inside the chambers can be stably controlled. Temperature control of the top and bottom plates of the chambers can be achieved by various means including circulating refrigerated baths, thermoelectric modules and heating wires. Accurate temperature measurement is equally important and can be achieved with the use of thermocouples and high accuracy meters. The high accuracy required for vapor pressure at the surfaces of top and bottom plates may be achieved with the use of ice covered surfaces under controlled temperatures.

A diffusion chamber with isothermal plates provides a central environment with only a single set of temperature and supersaturation. By producing a temperature gradient on one or both plates, a range of supersaturations and/or temperatures can be produced (Schaller and Fukuta, 1979; Fukuta and Saxena, 1979a and 1979b). Simultaneous exposure of ice nuclei to this range of supersaturation and/or temperature

makes possible a much more efficient and comprehensive study of the ice nuclei. In this manner, ice nuclei behaviors on a line instead of a single point on the supersaturation-temperature plane can be determined from a single sampling.

Most thermal diffusion chambers have a small height and consequently a small volume. Ice nuclei studies which require large smaple volumes cannot utilize such chambers. However, by creating a flow through the chamber, studying large volume of sample becomes possible (Sinclair and Hoopes, 1975). Caution must be taken to insure the flow is laminar so that the environment where ice nuclei activate can be accurately determined. Any turbulence in the flow would mix the sample air and the clarity of the condition for sample activation would be lost.

Wall effects (Elliott, 1971; Goroch and Carstens, 1972; Tomlinson and Fukuta, 1979) and transient supersaturations (Fitzgerald, 1970, 1972, Saxena et al., 1970) are important in designing a diffusion chamber with well-defined chamber conditions. Wall effects can be avoided by maintaining a large aspect ratio (width to height ratio) and avoiding the region close to the wall. Transient supersaturations must likewise be avoided since the momentarily high supersaturations activate some ice nuclei which otherwise would remain unactivated. Preconditioning of the sample can eliminate transient supersaturations in many cases (Saxena, et al., 1970). However, preconditioning is not always possible and a delay of the vapor diffusion can be used instead to avoid transient supersaturations (Fukuta and Saxena, 1979a).

Once the ice nuclei produce ice crystals, care must be taken that all the nucleated crystals are counted. Ice crystal counting in thermal diffusion chambers has been one of the crucial problems to be solved.

(Hallett, 1971). The new method developed in this study allows the crystals to be integrated on a special film. It is imperative that all the nucleated crystals be collected and not allowed to melt or sublimate prior to counting. It is equally important that no crystals will be produced by the collecting surface, i.e. the film will produce no background crystals. By taking these precautions, we insure that all the crystals seen on the collection film were nucleated in the chamber under the given environmental conditions.

Control and measurement of the air flow is another critical factor. Since the quantity to be determined by measurements is the number of active ice nuclei per unit volume, the volume of the sample must be accurately determined. The residence time of the sample also needs to be computed using the flow rate, because it is this residence time that dictates where and when steady state is reached in the chamber.

The new continuous flow horizontal gradient ice thermal diffusion chamber presented here satisfies all the requirements stated above. The chamber is designed with three primary sections, i.e., the prechamber, the main chamber, and the postchamber together with an intake device for proper introduction of the sample and an exit device for removing the air from the chamber.

3.2 Final Design and Construction

The chamber was constructed entirely in our laboratory. Copper was chosen as the basic metal material for top and bottom plates of the chamber for its good heat conduction, ease of fabrication by soldering, and rustproof properties. Plexiglass was utilized where an insulating material was required. It was selected for its ease of fabrication, reasonable strength, and transparency where observation into the

chamber was desirable. Figure 3 shows the basic design. Photographs of the entire chamber and support equipment are presented in Figures 4(a) and 4(b). The main parts are identified in Figure 5. In the following discussion, directions (left and right) are defined as facing downstream of the flow.

3.2.1 Sample intake device

The sample should be introduced and moved through a region of approximately constant temperature and supersaturation near the vertical center of the chamber while avoiding the regions close to the walls (Hudson and Squires, 1973). This positioning is achieved by sandwiching the sample with filtered air, i.e. air filtered of both cloud condensation and ice nuclei. The filtered air also separates the sample from the walls. This sandwiching of the sample is done with an intake device which is placed at the upstream end of the chamber. A photograph is presented in Figure 6(a).

The filtered air and the sample air enter the intake device from both sides to insure the horizontal uniformity of the layers as shown in Figure 6(b). Low angle wedges (fifteen degrees or less) are used for filtered air introduction into the chamber to avoid turbulence. Brass plates of 1/32 inch (0.8 mm) thickness are used in the construction and are glued with epoxy resin instead of soldered to avoid warpage. Shims of the appropriate thickness were used to obtain uniformity of the slit width during the construction. The slit openings are 1/16 inch (1.6 mm) for the filtered air and 1/32 inch (0.8 mm) for the sample air. The sides are made of 1/8 inch (3.2 mm) plexiglass, the right side kept clear for observation and the left side painted with flat black. The vertical position of the sample air can be controlled by

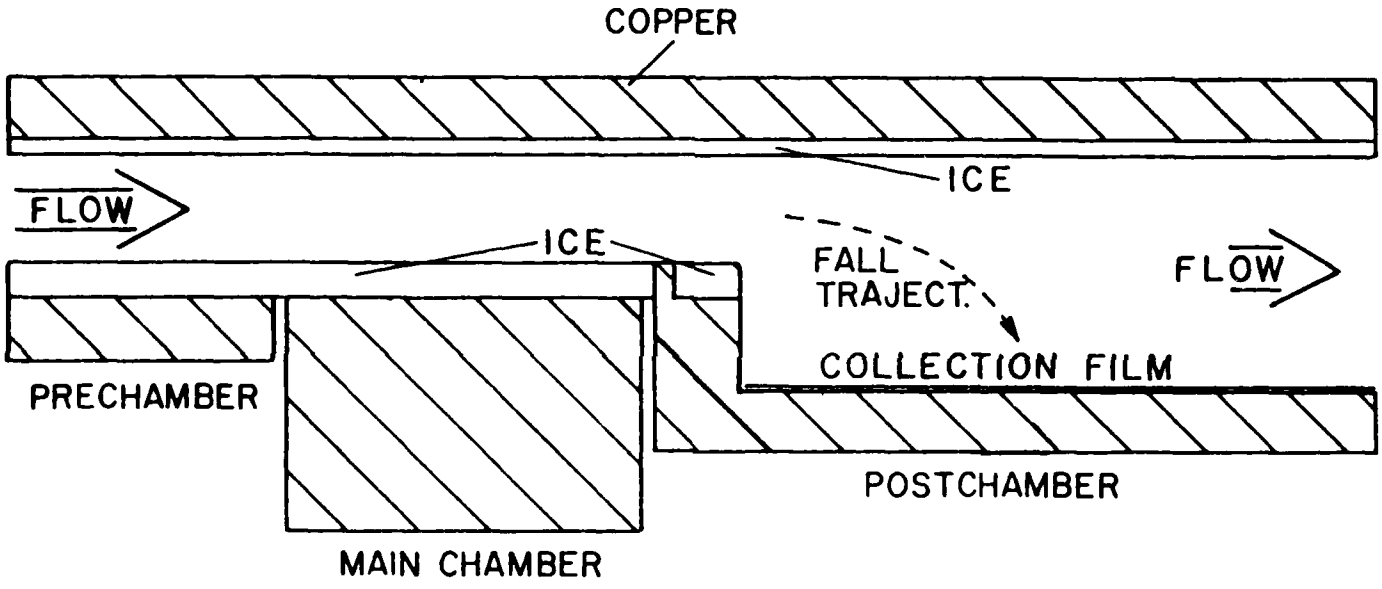

Figure 3. Design of the continuous flow ice thermal diffusion chamber. The height scale is expanded by a factor of 10.

Figure 4(a). Photograph of the entire chamber with the top removed and inverted behind the chamber.

Figure 4(b). Photograph of the support equipment including the flow-meters, the power supplies, the air pump, and the Terak computer.

(a)

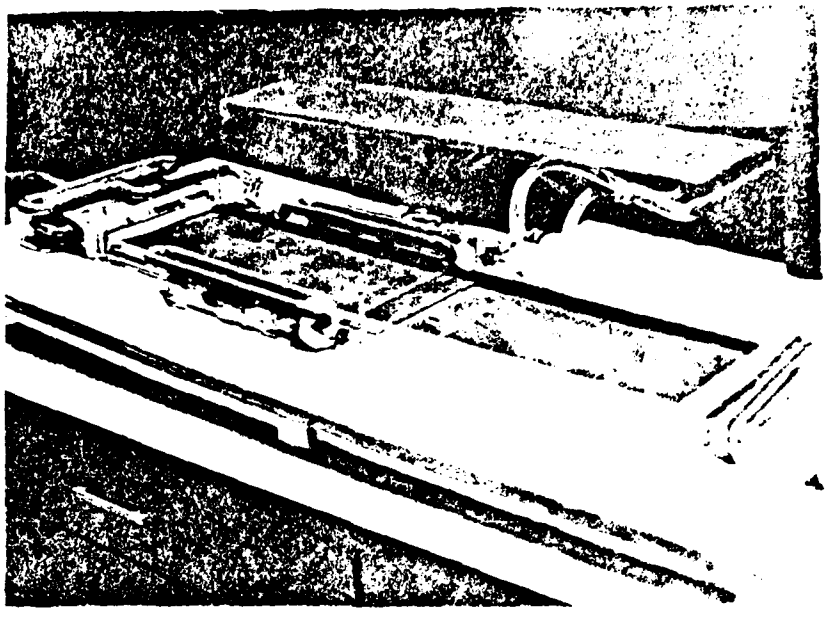

(b)

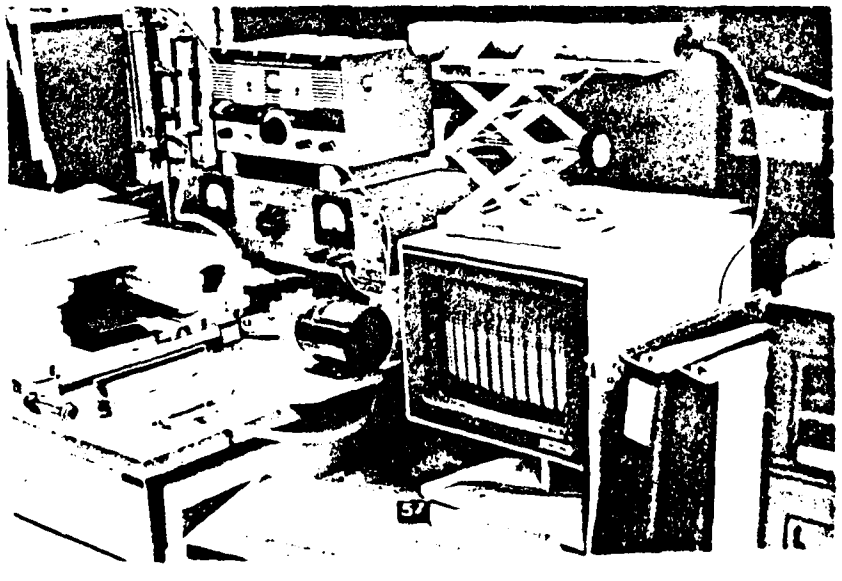

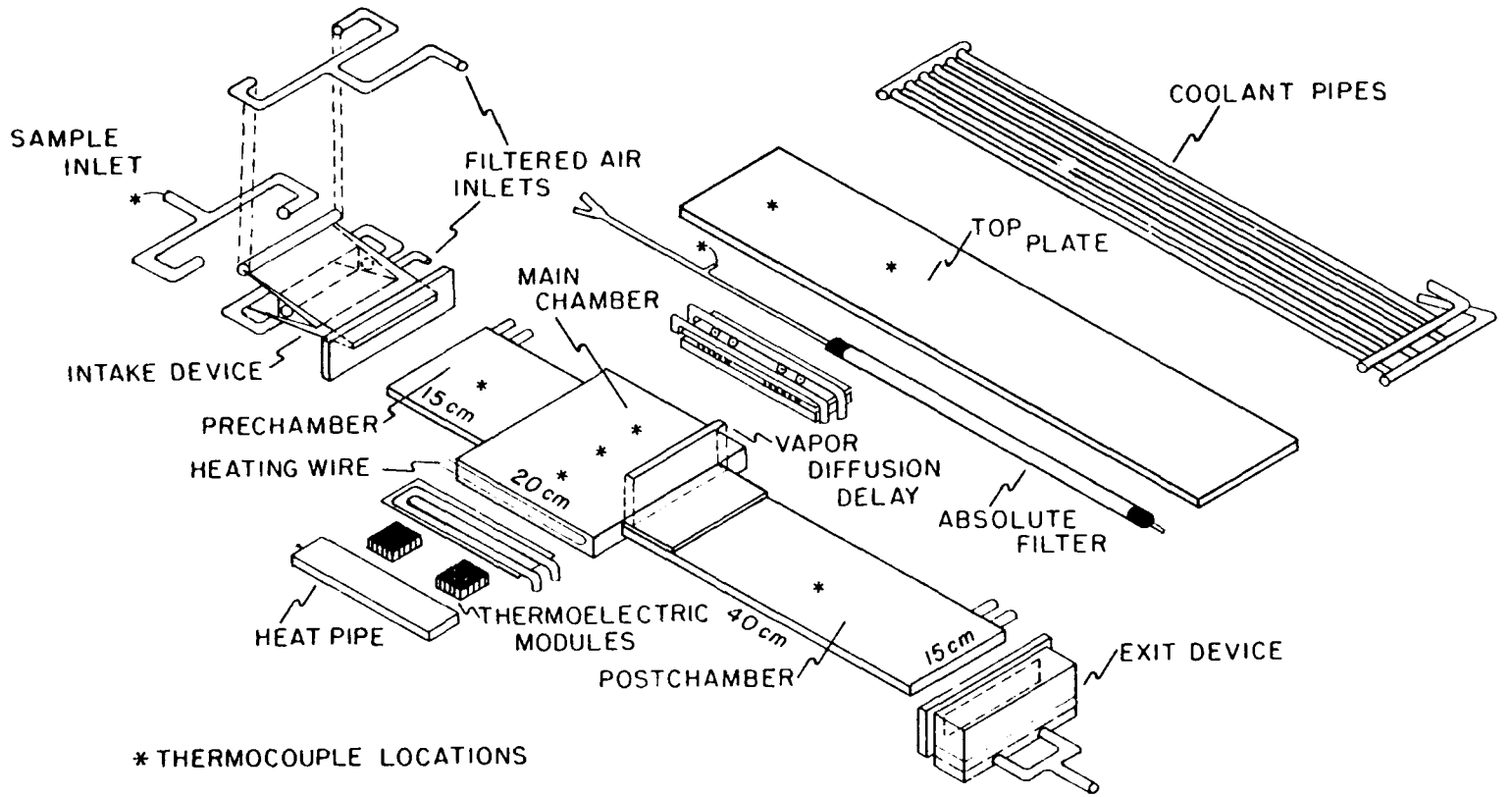

Figure 5. Expanded drawing of the complete chamber with the main components identified.

Figure 6(a). Photograph of the intake device before assembly showing the wedges used for sandwiching the sample air between the layers of filtered air.

Figure 6(b). Photograph of the intake device before assembly showing the symmetry used for the introduction of the filtered air and the sample to insure uniformity of the layers.

Figure 6(c). Photograph of a smoke test showing the uniformity and laminar flow of the sample air as it is sandwiched between layers of clear filtered air.

Figure 6(d). Photograph of a smoke test viewed from the exit end of the postchamber.

(a)

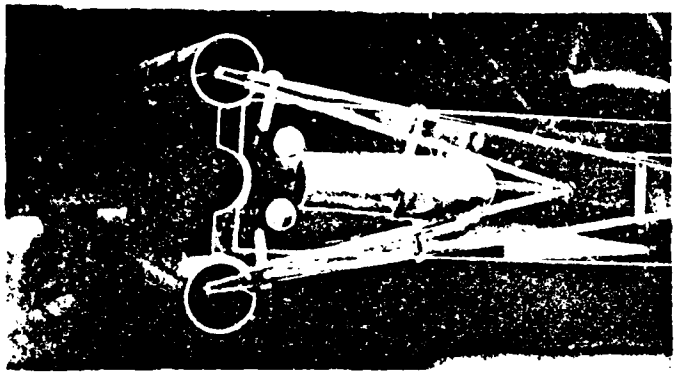

(b)

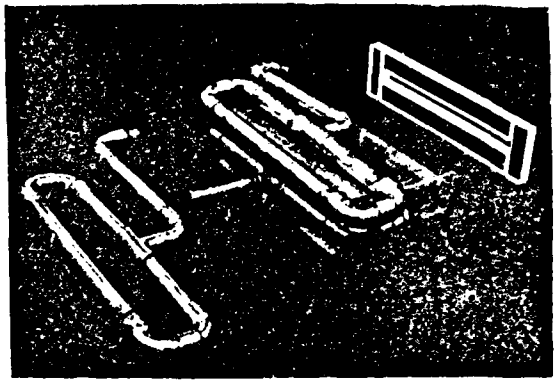

(c)

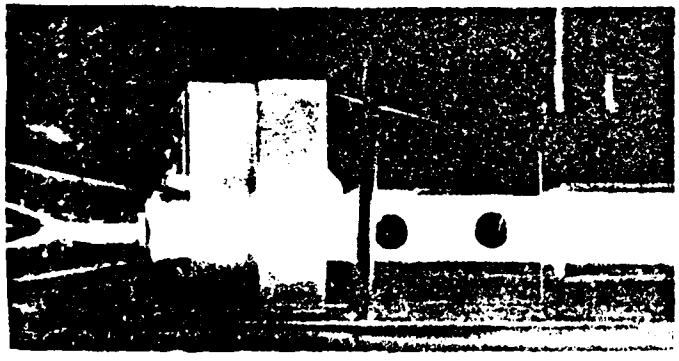

(d)

adjusting the ratio of the thicknesses of the filtered air above and below the sample. The thickness of the sample layer is adjusted by controlling its flow rate. The sample layer is separated from the walls by blocking the slit for approximately 2.5 cm adjacent to each wall. Smoke was used to verify the position and uniformity of the sample layer. Photographs of smoke tests are shown in Figures 6(c) and 6(d).

3.2.2 Prechamber

The role of the prechamber is to precondition the sample air so that transient supersaturations are avoided when the sample air enters the main chamber. The sample air is preconditioned approximately to the temperature and vapor pressure of the top plate (Saxena et al., 1970). Additionally, caution must be taken to avoid condensation in the sample air when the sample enters the prechamber. This is achieved by regulating the filtered air from the postchamber and warming it. Figure 7 shows the effect of this warming.

The prechamber shares the top plate with the other sections. The top plate is constructed of 1/8 inch (3.2 mm) copper plate with eight copper cooling pipes soldered on the top. The bottom plate is also 1/8 inch (3.2 mm) copper with a copper cooling coil attached to the bottom. The bottom plate is thermally insulated from the intake device by 1/2 inch (12.7 mm) plexiglass and from the main chamber by silicone sealant of 5 mm thickness. The side walls are constructed of 3.8 inch (9.5 mm) plexiglass with the right side kept transparent and the left side painted with flat black. The side walls are continuous through the remainder of the chamber. The walls are 9 mm high which, after 2 mm of ice is applied to the bottom plate and 1 mm to the top, give

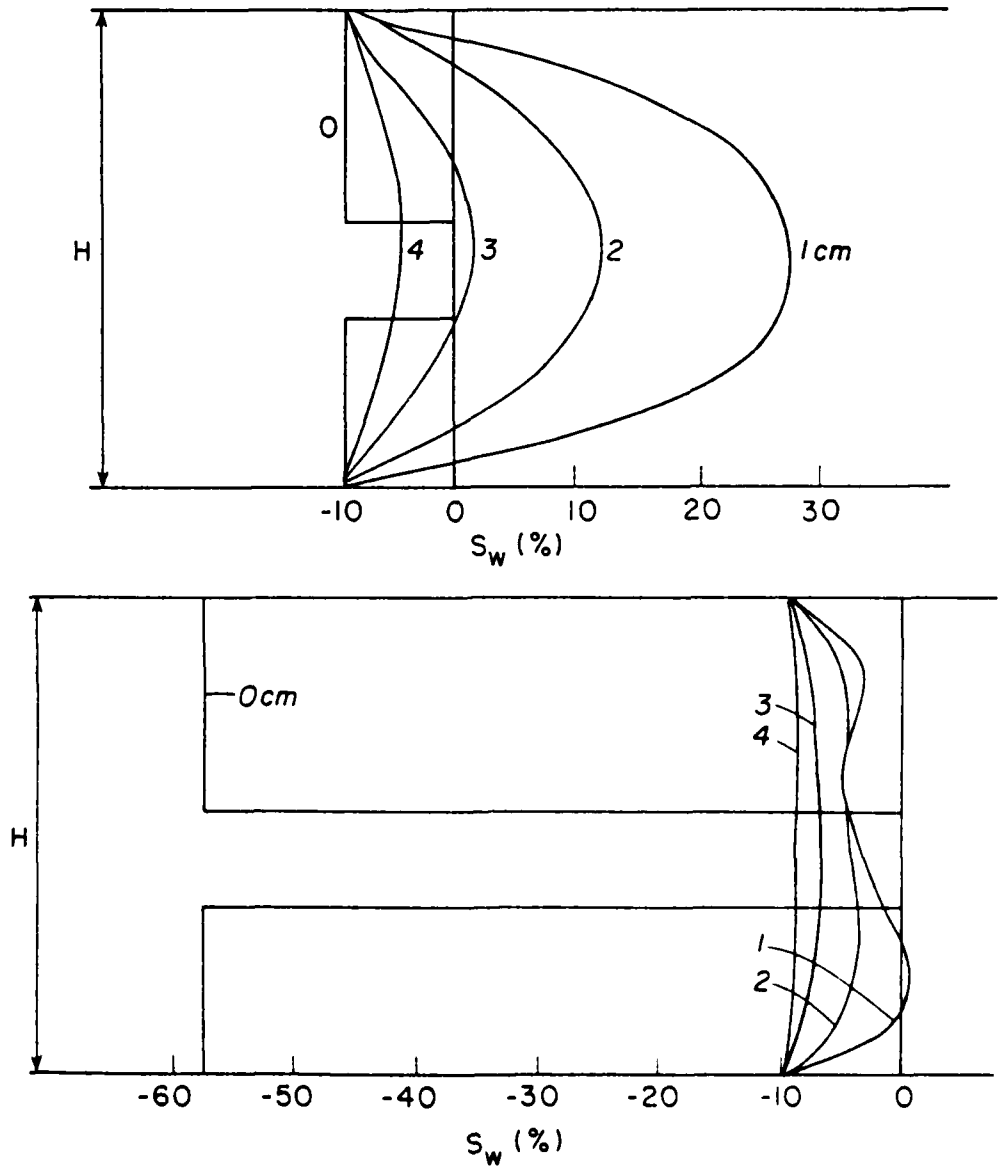

Figure 7. The effect of warming the recycled filtered air. (a) illustrates the use of filtered air at -10°C while (b) illustrates the effect of warming it to 0°C. The distances shown are from the entrance of the prechamber.

a 6 mm working height between the top and bottom ice layers. The 15 cm length of the prechamber allows the sample to reach steady state before entering the main chamber.

3.2.3 Main chamber

A range of environmental conditions are maintained in the main chamber for activation of ice nuclei. The shared top plate of the main chamber is held isothermal while a temperature gradient is maintained across the bottom plate. The result is a range of supersaturation across the horizontal median plane of the chamber with near isothermal condition.

The walls and top plate of the main chamber are the same as those in the prechamber. The bottom plate is 1/2 inch (12.7 mm) thick copper and extends 3 cm beyond the left wall and 4 cm beyond the right wall. The use of a thick plate at the bottom enables a near linear temperature gradient to be maintained across it. The bottom plate is insulated from the adjacent plates by a 5 mm width of silicone sealant. An angled mirror, placed just outside the right wall, allows observation of the interior of the main chamber while the chamber is in operation.

Heat pipes are utilized to insure temperature uniformity along the bottom plate in the direction of the flow (Dunn and Reay, 1978). In the heat pipes, methylene dichloride is used. The heat pipes are soldered to the edges of the bottom plate. The top surfaces of the heat pipes are cooled with thermoelectric modules which utilize antifreeze liquid from the circulating bath as a heat sink. The details of the heat pipe and thermoelectric modules installation will be discussed later.

The length of the main chamber is 20 cm. For reasonable flow

rates, this length is adequate for the sample air to reach steady state before exiting the main chamber. In most cases, steady state is reached for temperature and vapor fields in the first half of the chamber. Hence, steady state conditions are held for the last half. A cross-sectional drawing is presented in Figure 8.

3.2.4 Postchamber and exit device

The nucleated ice crystals are collected for counting in the postchamber. The new collection scheme utilized will be discussed in detail later. The collection scheme however requires the postchamber to be operated at warmer temperatures than the main chamber in order to avoid spurious ice nucleation on the ice crystal detection surface, i.e., a special film. Special precautions must be taken to avoid transient supersaturations since the incoming air from the main chamber is not preconditioned to the temperature and vapor pressure of the top plate. In order to avoid these transient supersaturations a bare metal surface is employed on the bottom plate at the beginning of the postchamber. In this manner, the heat conduction from the warmer bottom plate begins upward into the chamber air at the beginning of the postchamber while the water vapor diffusion process is delayed. The height of the postchamber is maintained at 6 mm for the first 5 cm of the postchamber before expanding to 12 mm over the collection film. This narrow height at the beginning allows the air to acquire quickly the temperature and vapor pressure profiles of the postchamber and thereby helps insure thermal stability of the air in the postchamber. The postchamber height expansion slows the flow and allows time for the crystals to settle on the collecting film.

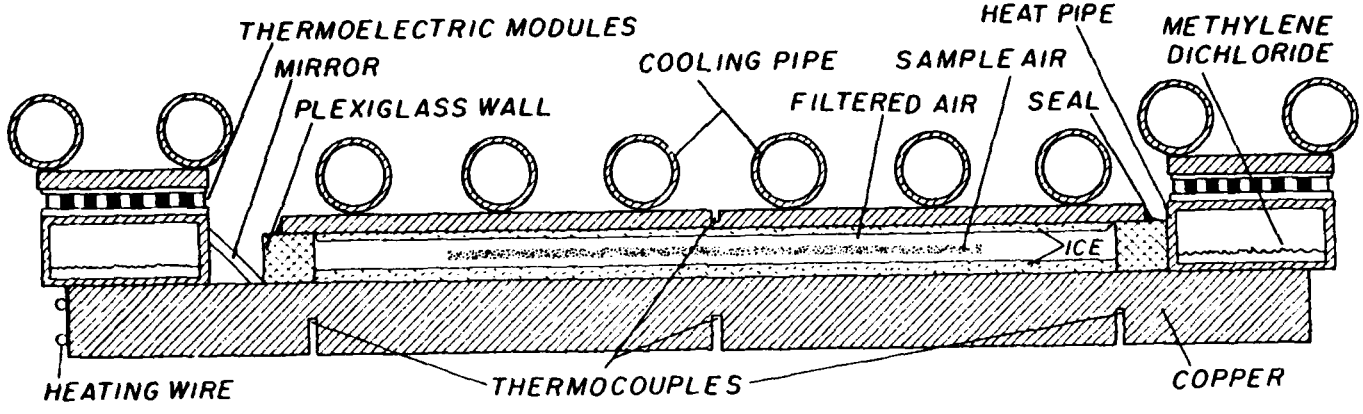

Figure 8. Cross section of the main chamber with the flow direction out of the page.

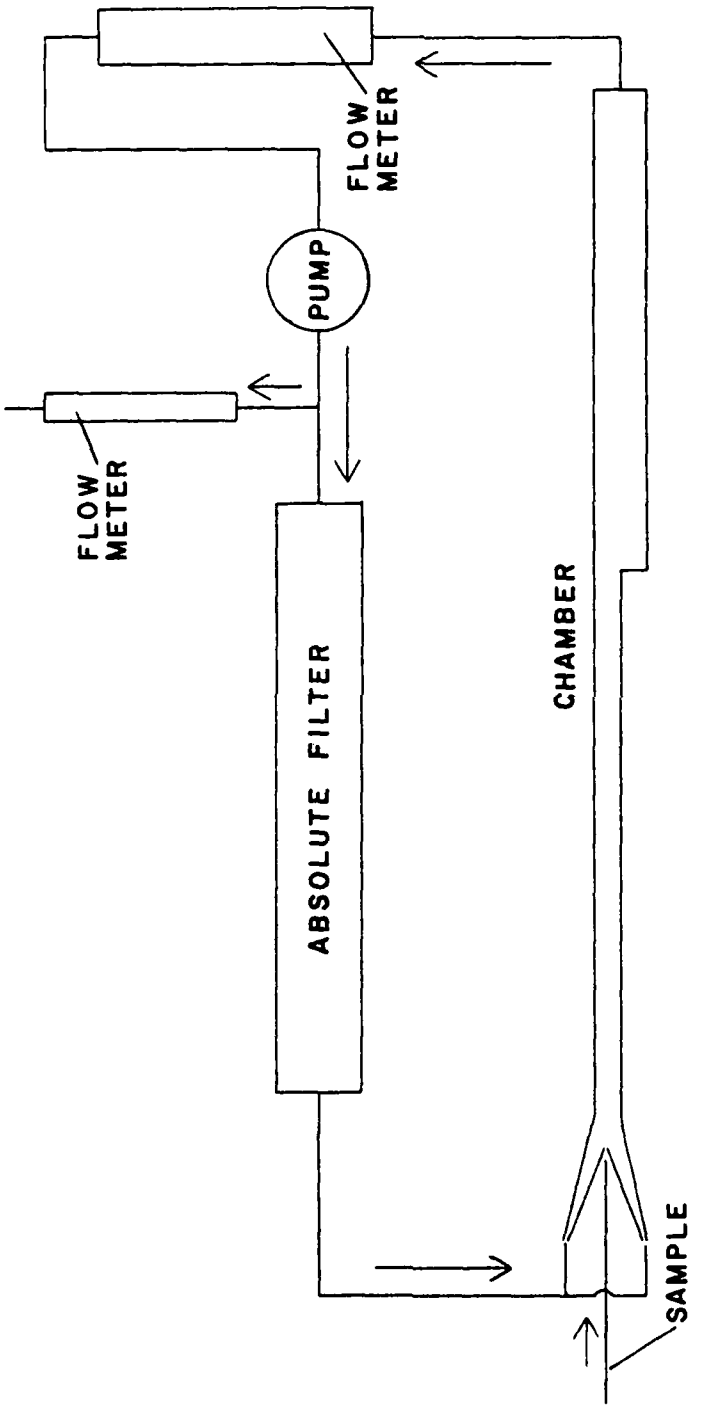

Figure 9. Schematic of the flow routing through the chamber and support equipment.

The side walls of the postchamber are continuous from the main chamber. The bottom plate is 1/8 inch (3.2 mm) copper with a cooling coil on the bottom. A 5 mm high by 5 cm wide copper block is soldered to the bottom plate at the beginning of the postchamber to achieve the narrow height at the beginning.

Air is removed from the postchamber through an exit device attached to the downstream end of the chamber. It is constructed of 1/8 inch (0.32 mm) plexiglass and the design allows observation into the chamber from the rear. The air exits through two pipes in the bottom, and a 1.5 cm layer of open cell foam equalizes the pressure gradient for uniform flow.

The filtered air used to sandwich the sample air is passed through an absolute filter which consists of a plexiglass cylinder 45 cm long and 2 inches (5.1 cm) in diameter with tightly packed glass wool. Since the vapor pressure of the filtered postchamber air is known, when it is recycled to sandwich the sample air, the transient supersaturation in the sample air can be computed from the vapor pressure value and accordingly controlled.

As stated earlier, flow control and measurement is crucial for the ice nuclei measurements in the present device. A schematic of the flow conditions is presented in Figure 9. The flow is measured by two flowmeters and accordingly controlled. After the air exits the chamber, it flows through a meter which measures and regulates the total flow, i.e., both sample and filtered air. The flow then goes through a Markson air pump, model 6363. As the air exits the pump, it is divided into two flows, one through the absolute filter for reuse in the chamber and the other through a second flowmeter into the environment.

By adjusting the flow through the second meter, the amount of sample introduced into the chamber is regulated. For example, when the second flowmeter is closed, the same air is recycled through the chamber thus creating a closed system with only filtered air entering the chamber. When the second meter is adjusted to a flow rate, say one liter per minute, air is bled from the system at a rate of one liter per minute and is replaced by sample air through the intake device at the same rate. In this manner, the sample air enters directly into the chamber without passing through a meter or a pump, thus avoiding any modification of the sample by these devices (Langer, 1971). The flow meters are Manostat and were calibrated with a Bubble-o-Meter in our laboratory.

3.2.5 Ice crystal detection

The detection and counting of the nucleated ice crystals in the ice thermal diffusion chambers has long been a problem (Alofs and Carstens, 1976). For thermal diffusion chambers, some types of optical or photographic detection scheme including the visual method using lasers or other light sources were employed. These methods are awkward and often unreliable even for studying artificial ice nuclei where the number of ice crystals formed can be controlled. The scarcity of natural ice nuclei eliminates these approaches entirely for their detection. Hence, a scheme which collects the ice crystals is required for accurate counting. In addition, a collection scheme which provides a number integration is preferred, especially for natural ice nuclei studies, i.e., a scheme where crystals nucleated under the same environmental conditions are collected in the same region for counting.

There are two critical requirements which must be met by any ice crystal collection scheme; that all nucleated crystals be received on the collection surface and that no additional crystals are produced by the collection surface. It was found that an acceptable collection surface under the temperature of the bottom plate in the main chamber was a difficult task. A spectrum of materials were tested, but all had significant but different problems. A variety of semipermeable membranes were tested being placed on the ice-coated bottom plate of the main chamber including polyurethane, cellophane, cellulose acetate and cuperphane (used in artificial kidney machines). Most were acceptable at warm temperatures but nucleated ice crystals on the surface at lower temperatures. Many fabrics were tested including silk, velvet, rayon, polyester, satin, cotton, and others. Even the closest weave was too coarse and allows crystals to either fall through or become obscured by the fabric. Tissue paper and carbon paper wrinkled badly whenever an ice supersaturation existed. Carbon black dispersed in ether was poured over the ice surface and after the ether evaporated, a carbon layer remained on the ice surface. This method however, besides being awkward to apply, did not leave a uniform layer of carbon black.

Mylar copy film was found to have many favorable characteristics. Until very cold temperatures are reached, the film does not nucleate ice crystals on the surface. The black surface offers a high contrast with the ice crystals under low angle illumination. The backing is nonpermeable with water vapor, a characteristic used to our advantage in the collection scheme. The film is hardy, readily available, and requires no special handling or preparation. The surface is smooth and does not wrinkle as does normal carbon paper. In addition, it was

found that the surface has a poisoning effect on the nuclei after the collected crystals melted and evaporated. This allows the film to be reused many times without fear of background crystal counts.

The film is adhered to a 1/32 inch (0.8 mm) aluminum sheet which can be easily slid into the postchamber from the rear. The film is removed from the postchamber after the crystals have been collected and put in a freezer for photographing of the collected ice crystals. Figure 10 shows the method of photographing. The film is then allowed to dry for reuse.

3.2.6 Temperature control and measurement

A Neslab circulating refrigerated bath, Model RTE-3, furnishes the temperature control for the top plate and the bottom plates of the prechamber and postchamber. Furthermore, it is used as a heat sink for the thermoelectric modules. The coolant, commercial antifreeze, is routed from the circulating bath, first through the coils on the bottom plates, then across the thermoelectric modules where heat is gained, and finally through the coolant pipes on the top plate. This routing scheme permits the top plate to stay at a temperature approximately one degree warmer than the bottom plates of the prechamber and postchamber and thereby enhances the thermal stability of the flow and secures a positive vertical vapor pressure gradient in the postchamber. In this manner sublimation of the collected ice crystals is avoided in the postchamber.

Cambion thermoelectric modules, model 2001, are used with the heat pipes for temperature control on the edges of the main chamber bottom plate. They are installed using thermal compound with the cooling sides in contact with the tops of the heat pipes and the warm side in

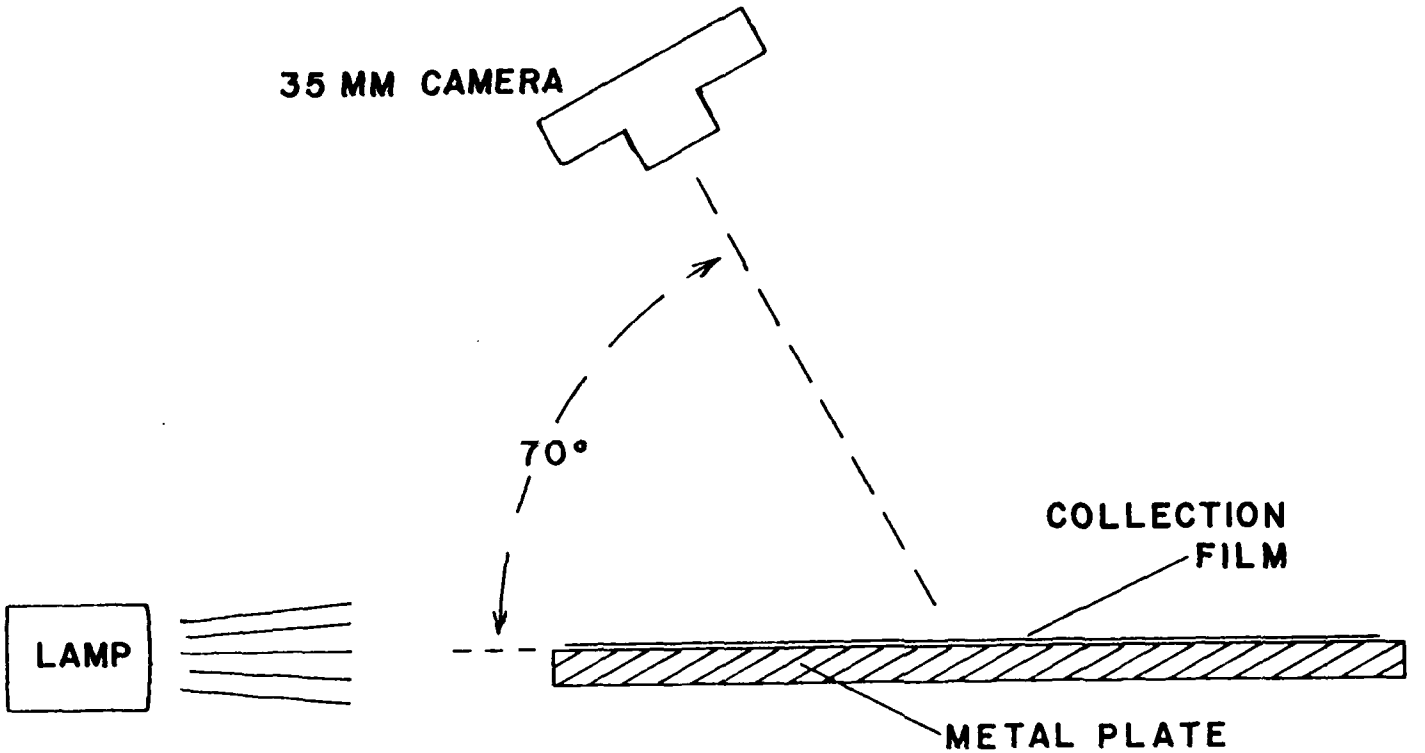

Figure 10. The arrangement for photographing the crystals on the collection film.

contact with a plate cooled by the coolant from the circulating bath. Four modules are used for the cold side and two for the warm side. The modules are wired in series and their output is controlled by adjusting the current through them. Separate DC power supplies are used for each side. In addition to the cooling modules, a heating wire is attached to the edge of the warm side to supply heat when required. The wire is a 40 cm length of 24 gauge constantan. The same power supply used for the thermoelectric modules on that side is used to heat the wire.

The temperature measurements are made by copper-constantan thermocouples with 24 gauge extention wires. The thermocouples were spot-welded to obtain a single contact between the two metals. A melting ice bath is used for the temperature reference. The voltage output of the thermocouples is measured using a Keithley digital voltmeter, Model 174. This combination produces an accuracy of 0.01°C at -10°C.

The temperature is measured at nine locations in the chamber. The temperature recording is automated and controlled by a Terak minicomputer. Each temperature is recorded every 25 seconds on a magnetic disk and shown on a video display screen. The temperature is measured at the following locations:

- Prechamber; middle of the top and bottom plates.
- Main chamber; half way down the length of the bottom plate at the left wall, middle of the chamber and right wall and at the middle of the top plate.
- Postchamber; middle of the bottom plate.
- Filtered air; just prior to the entrance into the intake device.
- Sample air; just prior to the entrance into the intake device.

The thermocouples which measure the temperature in the plates are painted with a solution of plexiglass to electrically insulate them from the copper plates. In addition, they were coated with thermal compound before being inserted into holes in the plates. The thermocouples which measure air temperatures are inserted directly into the air flow.

3.3 Chamber Operation

3.3.1 Application of ice surfaces

The ice surfaces on the top and bottom plates must be of uniform thickness and have smooth surfaces. Many methods for applying the ice were tested but most of them produced either non-uniform ice layers or ice layer with rough surfaces. Two different methods were finally chosen to apply the bottom and top ice layers. For the bottom plates, 110 cm^3 of water are poured over the bottom plates where ice coating is required. This gives a 2 mm layer of ice over these plates. Capillary action of the water keeps it from running off the front and near edges. The copper plate used at the beginning of the postchamber is placed in the water and frozen in place. As the plates are cooled, the water freezes in a uniform layer with a smooth surface.

For application of the ice layer on the top plate, the top plate is inverted and tape placed along the outside 5 mm of each side. Next the plate is cooled to -5°C. Water is applied to the surface using a sponge covered with a plastic mesh like those used in service stations to clean automobile windshields. The thin water layer applied soon freezes. The procedure is repeated until a 1 mm layer of ice builds up. Then, the tape is removed while moving the wet sponge along

the tape and warming the ice. This procedure prevents any chipping of the ice. This ice-free area on the edges where the tape is removed, is used to create a leakproof seal with the top of the side walls. Figures 11(a) and 11(b) show this ice application scheme.

3.3.2 Sandwiching of the sample

The main chamber is supersaturated with respect to ice throughout the interior except on the boundaries where ice saturation is maintained. The ice supersaturation, however, is not constant vertically between the top and bottom plates but ranges from zero at the boundaries to a maximum near the center. For sufficiently large temperature differences between the plates, supersaturation with respect to water occurs with a maximum also near the center but not necessarily colocated with the maximum for ice supersaturation. However, for a thin sample layer around the center, both ice and water supersaturation are nearly constant at values close to their respective maxima.

The temperature varies almost linearly between the plates of the main chamber. Hence, within the thin sample layer, the temperature varies little. The thinner the layer, the less the variance of the temperature through the layer. Therefore the sample should be confined to as shallow a layer as possible for near isothermal conditions. However, there is a practical limit on the thickness of the layer since, as the sample layer thickness is reduced, the volume sampling rate becomes reduced. Thus, for a given sampling rate, there is a corresponding minimum sample layer thickness.

Under the shear flow condition of the chamber, the velocity varies from zero at the boundaries to a maximum at the vertical center. At

Figure 11(a). Application of the ice layer on the top plate at -5°C.

Figure 11(b). Removal of the tape along the edge of the top plate where an ice-free surface is required for contact with the side wall.

(a)

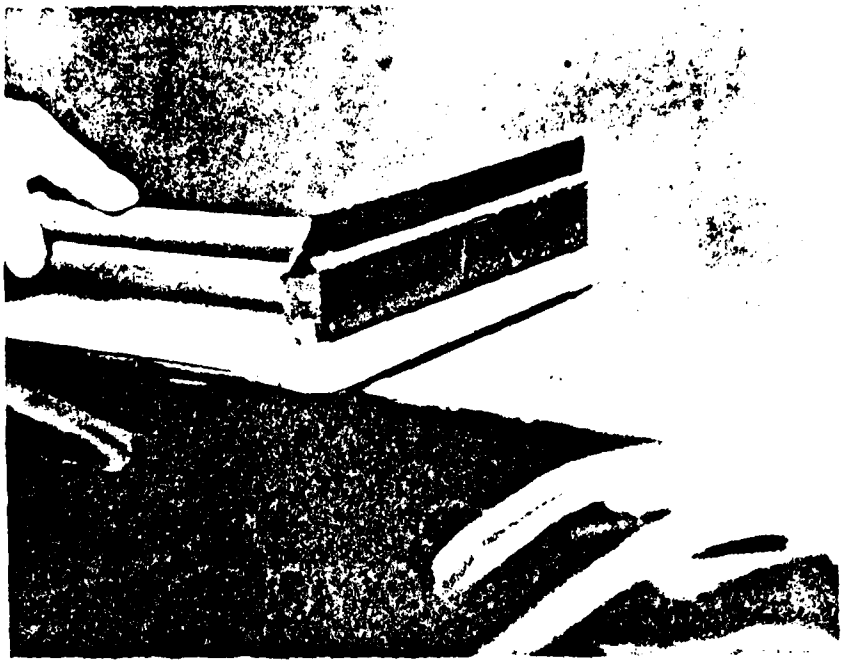

(b)

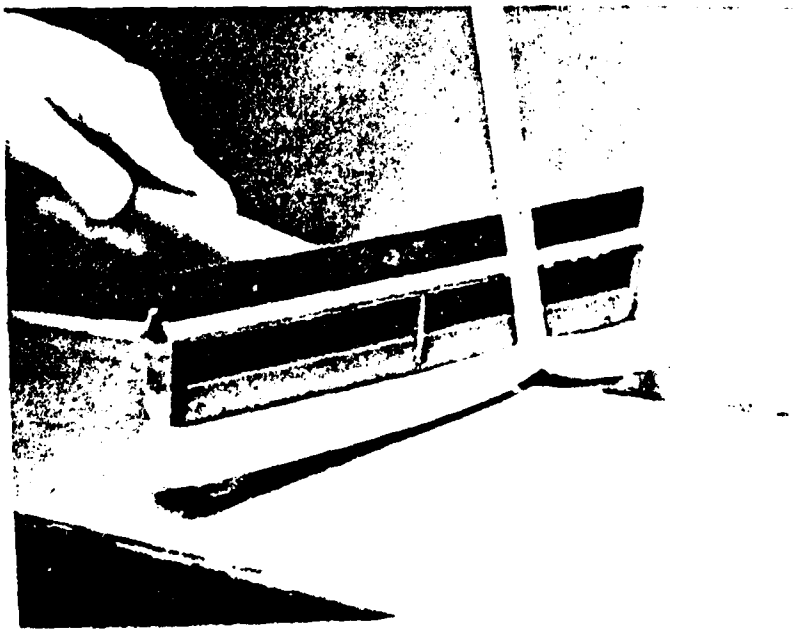

the center of the flow there exist a thin region where the flow velocity is nearly constant at the maximum velocity rate. Therefore, if the sample is confined to this thin region near the center of the chamber, it will be exposed to nearly uniform fields of supersaturation, temperature, and velocity. As discussed earlier, the temperature and water vapor fields and therefore the supersaturation can be accurately controlled and the velocity field can be computed.

The correct positioning and depth of the sample layer is done by means of the intake device described earlier. By controlling the relative thickness of the filtered air layers, the vertical position of the sample layer between the plates can be adjusted. The thickness of the sample layer is controlled by adjusting the bleed air through the second flow meter so that the desired sampling rate is achieved. The vertical position of the sample layer is adjusted to the region where the supersaturation, temperature, and velocity fields are nearly constant. Figure 12 illustrates the profiles of these parameters and the positioning of the sample. The intake device also introduces the filtered air between the sample air and the wall so that wall effects are avoided.

3.3.3 Preconditioning of the sample

Caution must be taken to insure that condensation does not occur in the sample air prior to entering the main chamber since condensation could alter the number of ice nuclei in the sample or modify their behavior by providing an uncontrolled opportunity for the liquid phase to build up on them. Since the temperatures of the filtered and the sample airs are measured, if the vapor pressure of the sample were known,

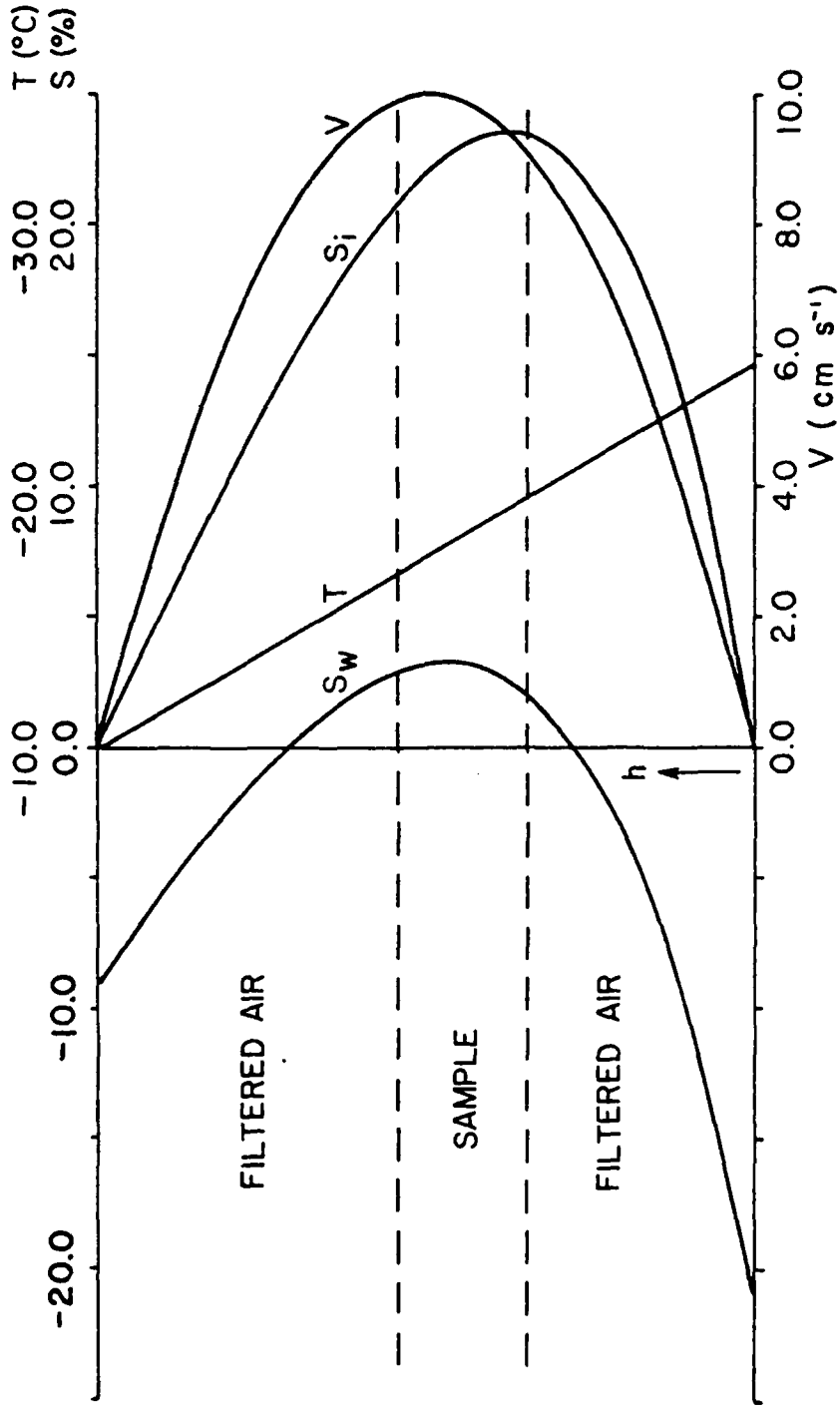

Figure 12. Sandwiching of the sample between layers of filtered air in the region where S_w, S_i, and V are nearly constant.

computations using the diffusion equation with advection could determine if water saturation were ever reached. Instead of using an additional device for measuring the vapor pressure of the sample air, we assume a water saturated sample and proceed with the calculations. Under conditions where transient water supersaturations are predicted to occur, the filtered air is heated properly to avoid them. By heating the filtered air, the temperature field of the predried filtered air remains sufficiently high while the vapor diffuses into it so that water supersaturation does not occur. This effect was previously shown in Figure 7.

The purpose of the prechamber is to precondition the sample to a temperature and a vapor pressure close to those of the top plate. This preconditioning prevents transient supersaturations from happening in the sample air when entering into the main chamber. The final condition attained in the prechamber is slightly different from isothermal since the top plate is held about 1°C warmer than the bottom. However, our computations show that this preconditioned profile is adequate to avoid transient supersaturations.

3.3.4 Activation of ice nuclei

The sample moves through a region in the main chamber where the supersaturation and temperature are known. The residence time is sufficient for the ice supersaturation value of the sample air to come within 10% of the steady state value. In most cases, this is accomplished in the first one half of the main chamber length. Therefore, the sample air stays within 10% from the steady state value of ice supersaturation for the last half of the main chamber. It is in this region where ice nucleation occurs in the sample air. With the horizontal variation of

supersaturation across the chamber, the ice nucleations which occur at different positions across the chamber have correspondingly different supersaturation thresholds.

The nucleated crystals are carried out of the main chamber by the flow and settle on the collection film in the postchamber. We stratify the horizontal supersaturation variation by defining lanes of nearly constant supersaturations horizontally across the flow. The lanes extend down the main chamber and into the postchamber. Because laminar flow is maintained, the crystals collected on the film in each lane must have nucleated at the supersaturation and temperature of that lane in the main chamber.

3.3.5 Collection of the ice crystals and analysis

The purpose of the postchamber is to collect the ice crystals which nucleated in the main chamber. There are two levels of the bottom plates in the post chamber; the first maintains the same level between ice layers as the main chamber and the second is lower so that the flow slows down there and crystals have time to settle on the film before the sample air exits the chamber. The temperature profile in the postchamber is the same as that in the prechamber, i.e. the bottom plate is maintained about 1°C colder than the top plate. This profile increases the thermal stability of the air and maintains a downward flux of vapor so that the collected crystals do not sublimate. This arrangement may lead to problems; as the cold air from the main chamber moves over the warm bottom plate of the postchamber, thermally unstable conditions can result. Furthermore, the air adjacent to the bottom plate in the main chamber has a very low vapor pressure and when it

moves to the postchamber, it can sublimate the collected crystals unless the vapor pressure is increased. This cold dry air can also evaporate or freeze the water droplets deposited on the collection film. For these reasons, the first 5 cm of postchamber are maintained at the 6 mm height with both the top and bottom plates covered with ice. This small height suppresses the thermal instability by making the temperature field reach the new steady state more quickly and reducing the available time for thermal instability. It also permits the vapor field of the air to reach the postchamber profile. The length of this ice covered bottom surface must sufficiently be short, however, so that nucleated crystals fall on the collection film instead on the ice surface.

The movement of this supersaturated cold air into the relatively warm postchamber will induce undesirable transient supersations unless precautions are taken (Fitzgerald, 1970; Saxena et al, 1970). These transient conditions occur because the vapor diffuses faster than the heat conducts. To avoid this problem, the vapor diffusion is deliberately delayed at the beginning of the postchamber while heat conduction proceeds in the air. This delay is acheived by substituting bare (non-ice covered) a copper strip for the ice layer on the bottom plate at the beginning of the postchamber. Computations show this procedure is adequate for avoiding supersaturations.

The Mylar copy film for ice crystal collection is used by adhering it to a 1/32 in aluminum plate with Scotch double-coated tape. It is introduced into the postchamber by sliding from the rear. When the temperature of the postchamber is above -10°C, best results are obtained by using a pretreated Mylar copy film which carries condensed water

droplets. The pretreatment procedure is as follows; the Mylar film is placed under a plexiglass cover which has wetted filter paper adhered to the interior. The cover is kept at room temperature. The film and the cover are placed on a thick metal plate precooled in a freezer. The film cools first and vapor diffuses to the film surface from the filter paper of the cover. The film becomes coated with small supercooled water droplets. When the postchamber temperature is below -10°C, the film should be used without pretreatment.

In order to confirm that the Mylar film produces no crystals on its surface, blank tests were run using only filtered air in the chamber. The tests consistently produced no background ice crystals on the film. This confirmed that the ice crystals collected during ice nuclei sample tests were indeed a result of ice nucleation in the main chamber.

An Olympus 35 mm OM-1 camera was used for recording ice crystals on the Mylar film and their subsequent analysis. After a sufficient sample volume is drawn through the chamber and the ice nuclei are activated, the film is placed under a thin plexiglass cover whose interior is coated with ice and is then moved to a freezer for photographing. The plexiglass cover protects ice crystals on the film while transferring to the freezer. The film is placed on a metal plate in the freezer held at about -10°C. If the crystals are not large enough to photograph, the film is placed under a plexiglass cover 1 cm high with wetted filter paper adhered to the interior to grow the crystals to easily recognizable sizes. The cover is kept at room temperature. When the crystals become sufficiently large, they are illuminated with a lamp at a low angle. The crystals are photographed at about a 70 degree angle

from the plane of the film. The photographing arrangement was previously shown in Figure 10.

After the photographs are developed, the lanes and their supersaturations are identified using an overlay. The number of crystals in each lane is determined and recorded. These number counts combine with the computed temperature and supersaturation fields are used for data analysis. An example of the collected crystals is presented in Figure 13(a) and the use of the overlay shown in Figure 13(b).

Another source of disturbance in the flow was dendrites grown on the bottom plate of the main chamber. This dendrite growth is not unexpected since a continuous downward flux of vapor exist as well as ice supersaturation above the bottom plate. These crystals protrude into the chamber interior and can disturb the laminar flow. These disturbances were confirmed with the smoke tests.

Two precautions are taken to eliminate this dendrite growth. First, whenever the chamber is cooled to operating temperatures and not in use, a plastic sheet is inserted between the plates. The dendrites then grow on the sheet and are removed from the chamber with the sheet before measurements. However, while the chamber is used for sampling, crystals do begin to grow on the bottom plate. These crystals are melted periodically by moving a warm copper plate over the surface. The plate is thermally insulated from the top ice surface completely and only exposed to the bottom surface for 1 cm of its 10 cm length. This design permits good control of the dendrite melting process. The short exposed length of the copper plate permits a quick melting and refreezing of the crystals, thereby leaving a smooth surface after melting no more ice layer surface than necessary.

Figure 13(a). Example of the received ice crystals on the collection film. The sample was silver iodide.

Figure 13(b). Use of the overlay dividing the collection film into lanes. The number of collected ice crystals in each lane is counted.

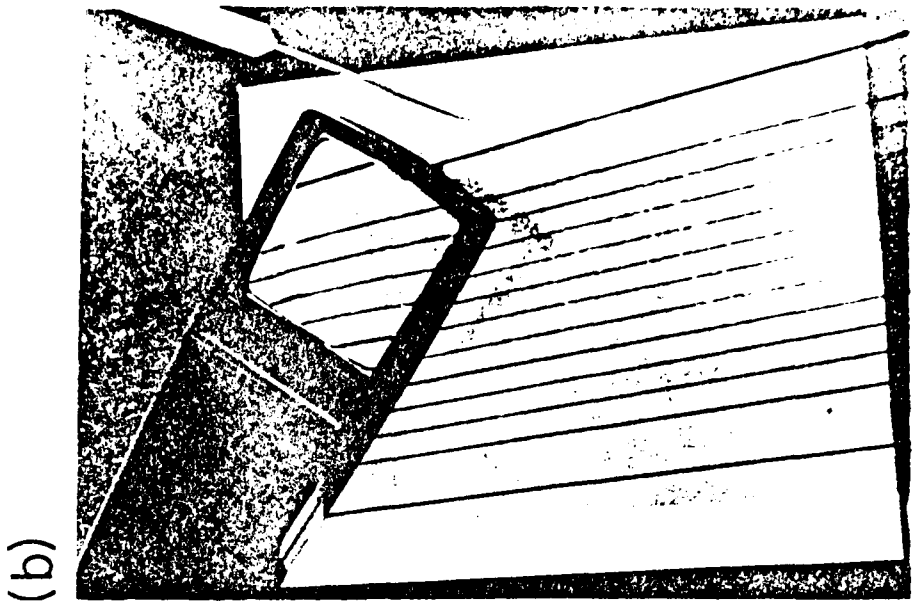

(b)

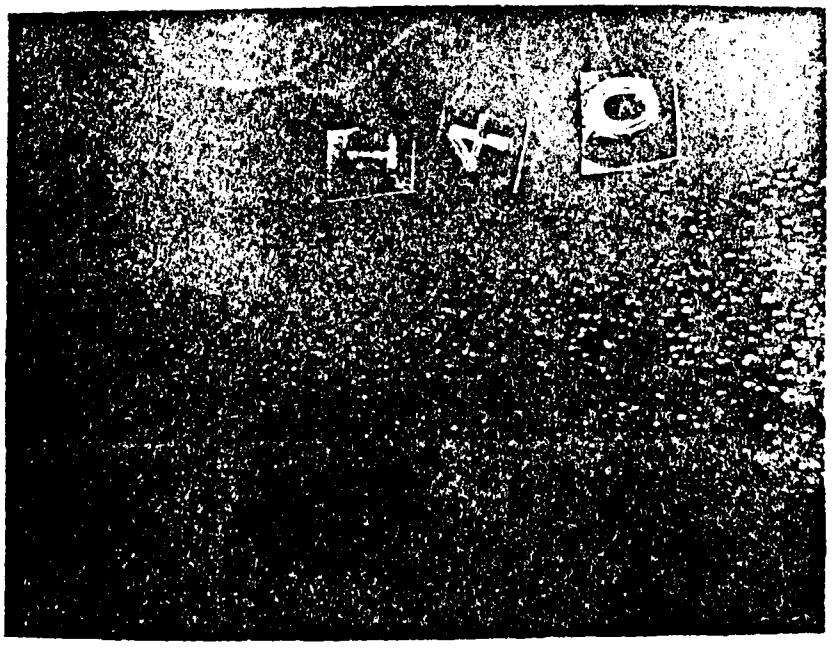

(a)

The shear flow velocity profile resulting from the presence of the top and bottom plates has been previously discussed. Shear flow also exists along the side walls, although its depth of penetration into the chamber is small. This velocity shear induces significant thermal instability along the walls. The air adjacent to the wall moves more slowly than that of the interior and therefore requires a shorter distance down the chamber to stabilize. Consequently, in the prechamber and main chamber, the air close to the wall becomes colder than that of the inner flows and causes subsidence along the wall. In the postchamber, the situation is vice versa; air close to the wall warms faster and convection occurs at the wall. The height of the main chamber was originally built to be 1 cm and that of the postchamber 2 cm. For these heights, the thermal instabilities along the walls were very large. In the postchamber, the air adjacent to the wall at the entrance was carried halfway across the top plate by the time it exited the chamber. A photograph of a smoke test showing this instability is given in Figure 14(a).

The solution to this problem was twofold. First, the heights were lowered to 6 mm and 12 mm, respectively, in the main chamber and postchamber so as to reduce the subsidence or convective force as well as its duration. This alone eliminated most of the instability but as can be seen in Figures 14(b) and 14(c), sample air at the wall is subject to some remaining convective forces. However, the width of the filtered air separating the sample from the walls was also increased slightly to insure that the sample air stayed out of any additional instability. These precautions proved adequate for maintaining laminar flow in the sample layer as was previously shown in

Figure 14(a). Photograph of a smoke test where the sample layer extended to the wall. A plexiglass plate is substituted for the top plate and the chamber is viewed from above. The air flow is from left to right.

Figure 14(b) and (c). Photograph of a smoke test viewed from the exit end of the chamber. The sample layer extended to the wall. The smoke is illuminated at the entrance to the postchamber in (b) and at the end of the post-chamber in (c).

(a)

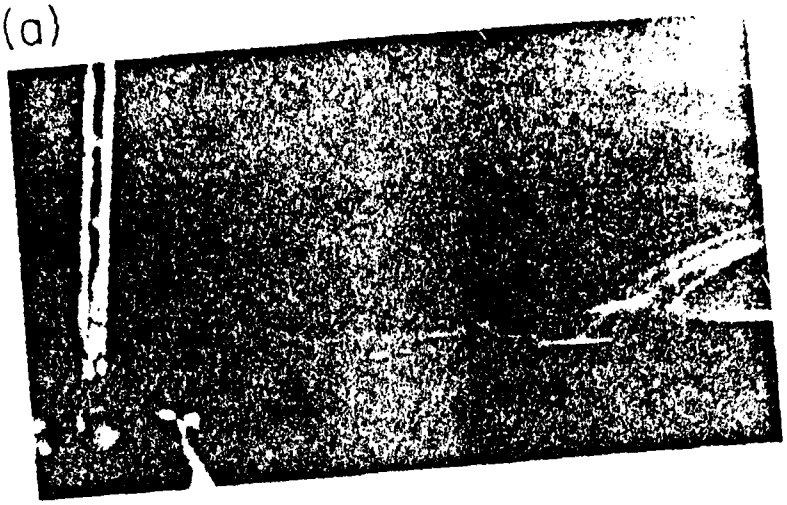

(b)

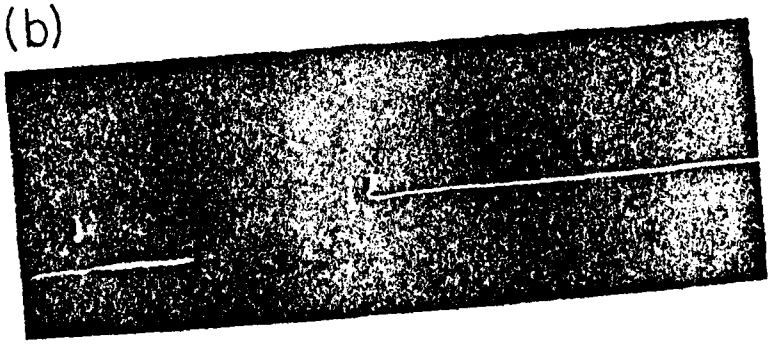

(c)

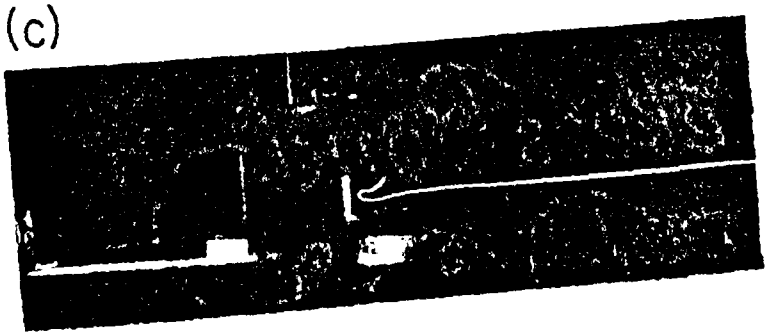

Figure 9.

A more obvious source of turbulence would be leaks in the chamber. All parts which are not routinely removed were sealed when they were installed with either foam strips or silicone rubber sealant. The top plate and the exit device are routinely removed. The top plate is sealed by applying a water bead along the edges. This bead quickly freezes to form an ice seal. Closed cell foam weather stripping is used to seal between the exit device and the postchamber. Smoke tests confirm the leakproof sealing of the chamber and the laminar flow throughout the chamber as shown in Figure 15(a) and 15(b).

3.4 Wall Effect Determination

Effects of side walls on the temperature and vapor fields, and therefore the supersaturation fields have long been recognized as a significant problem in thermal diffusion chambers (Elliott, 1971), but only recently have quantitative calculations been carried out to determine the penetration depth of the effects into the interior of the chambers. These wall effects are attributed to the ice saturated condition on the walls due to formed ice crystals on them, i.e. the near linear vapor pressure profile of the interior curves to the saturation values on the walls. Computations similiar to those presented in the paper by Tomlinson and Fukuta (1979) were carried out for the rectangular geometry of the present ice thermal diffusion chamber. The wall effects were included in every computation of the temperature and supersaturation fields, i.e. for each sample taken, the complete calculation was made using the measured temperatures. In this manner, accurate values for the temperature and supersaturation in the region

Figure 15. Photograph of a smoke test where the top plate was replaced with plexiglass. In (a), pressure waves were created by tapping the top of the intake device and the wave fronts were observed as they were advected downstream by the flow. In (b), smoke was released through pinholes in a straw across the entrance to the prechamber and the flow pattern of the smoke lines was observed.

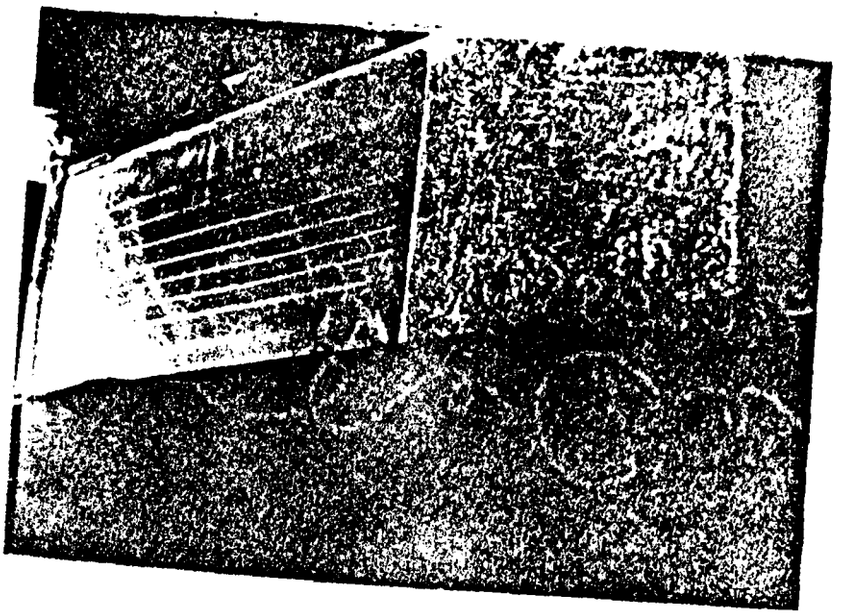

(a)

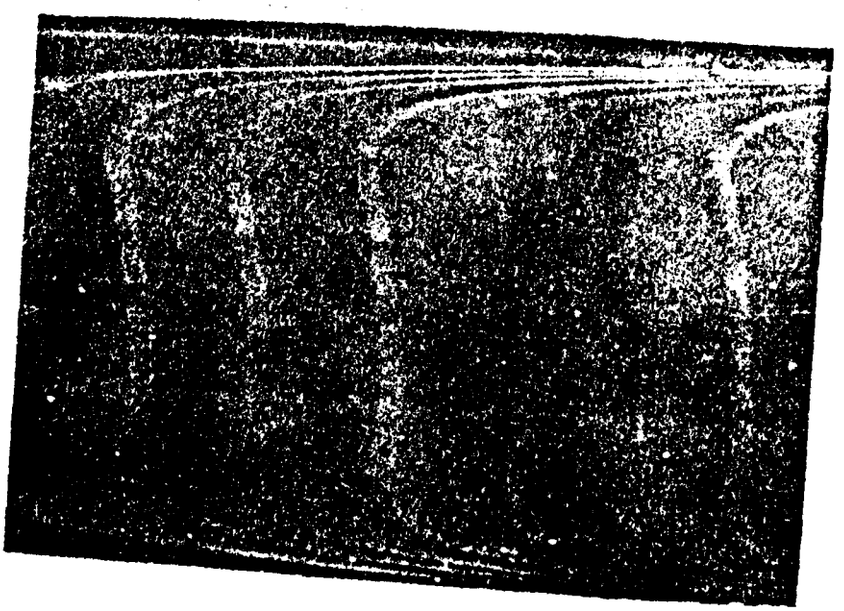

(b)

where ice nucleation occurs are obtained. Appendix A includes the equations and method used for these computations.

3.5 Error Analysis

The errors which are present in the chamber are due primarily to those in temperature measurements. As mentioned earlier, the error in temperature measurement with the equipment used is 0.01°C at -10°C. The temperature of the chamber was normally very stable when cooled to steady state. Small drifts were sometimes observed to occur, but were limited to ±0.02°C. For the error analysis, the value of ±0.03°C is used. Trial runs were made using the extremes of the temperature errors. The following ranges of relative error were determined:

$$18 - 30\ \%\ \text{for}\ \ 0.0 \leq S_w(\%) \leq 1.0$$

$$10 - 18\ \%\ \text{for}\ \ 1.0 \leq S_w(\%) \leq 5.0$$

$$1 - 2\ \%\ \text{for}\ 12.0 \leq S_i(\%) \leq 25.0$$

The errors associated with the wall effect have been determined and accordingly the sample air removed from the affected region. Therefore, there is no wall effect error in the sample. The computational errors are small compared with the above ranges of error and are negligible.

CHAPTER 4

NUMERICAL MODELING OF THE CHAMBER OPERATION

A detailed knowledge of the conditions throughout the chamber interior is essential in order for any meaningful detailed studies to be carried out. Numerical models which simulate the conditions can furnish the needed knowledge if the boundary conditions are properly described under steady state. Two such models have been developed for use in this study. The first computes the steady state conditions in vertical planes perpendicular to the flow direction. The other computes the steady state conditions in vertical planes parallel to the flow direction. The mathematical approaches used in these models are quite different but their computed fields agree very well along lines where the planes of each model intersect, indicating consistency of both models.

4.1 Model Describing the Chamber Conditions under Steady State and Wall Effects

The first numerical model was designed to compute the steady state conditions in a plane perpendicular to the flow with considerations given to wall effects. Twomey (1963) concluded that the influence of the side walls on the interior fields of the chamber must be considered when computing the fields. The present approach is similiar to that presented by Tomlinson and Fukuta (1979) but employs rectangular geometry for the chamber. As discussed in the latter paper, the models assumes wettable walls made of a thermal conductor. Vapor pressures values were used instead of vapor density for better accuracy as

suggested by Katz and Mirabel (1975).

For the steady-state transportation of water vapor without sources or sinks, the Laplace equation for vapor pressure $\nabla^2 P = 0$ holds with sufficient accuracy (Fukuta and Saxena, 1979). The approach for T and P computations is as follows: Since P is of an additive nature, the solution of the Laplace equation for P under the original boundary conditions is broken down into five component pressures satisfying boundary conditions (1) through (5) in Figure 16 (Carslaw and Jaeger, 1959) and the Laplace equation for each of them is solved separately and the solutions are added later. On the left wall,

$$P_L(z) = P_{BL} \exp\left[\frac{L}{R_V}\left(\frac{1}{T_{BL}} - \frac{1}{T_L(z)}\right)\right] ,$$

where L is the latent heat of sublimation per gram water and R_V the specific gas constant for water vapor, T_{BL} the temperature on the left side of the bottom plate and $T_L(z)$ the vertical temperature profile on the left wall. A similiar equation holds for the vapor pressure profile on the right wall. The vertical temperature fields on both walls and therefore interior of the chamber are assumed to be linear. The equations and procedure used for solving for each component pressure P_1 through P_5 is presented in Appendix A.

The solution for the Laplace equation for temperature under a linearly changing vertical wall temperature profile is simply a linear function of z. The saturation vapor pressure P_s is computed using the sixth degrees polynomials from Rasmussen (1978). The vapor pressure P at any point inside the chamber is given by

$$P(x,z) = P_1 + P_2(x,z) + P_3(x,z) + P_4(x,z) + P_5(x,z).$$

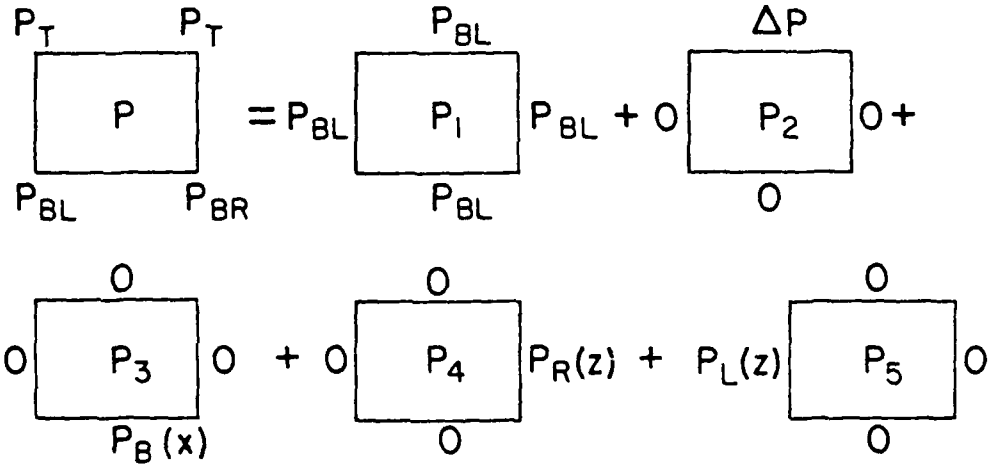

Figure 16. The components of water vapor pressure which are summed to reproduce the entire boundary conditions of the vapor pressure in the present chamber.

Using this pressure and the computed saturation vapor pressure, the supersaturation fields are computed for the chamber interior. In turn, these fields are used to determine the extent of the wall effects.

This model was run for the ranges of temperatures used in this study. It was found that the effects of the walls were confined to within 1.5 cm of the walls, i.e. the supersaturation values were within 10% of the infinte parallel plates value for all points further than 1.5 cm from the walls. Based on this model, it was decided that no sample air should be placed closer to the walls than 1.5 cm.

The measurements taken from the chamber during experiments indicated that although a thick copper plate was used for the bottom, deviations from a linear temperature profile were evident on it. Since the temperature is measured at three locations across the plate, a quadratic function is used to describe the temperature profile. This should give a good approximation to the actual temperature profile and the accuracy of the model is preserved.

The model is run for every experiment, thereby eliminating the requirement that the temperature be regulated exactly to some preset set of values for which the model has been previously run. The temperatures measured for each experiment yield computed sets of fields. The model requires approximately 25 minutes to run on the Terak for each set of experimental data and computes the following fields:

1) Temperature
2) Vapor pressure
3) Ice supersaturation
4) Water supersaturation
5) Error (or deviation) from the infinite plate case for ice

supersaturation

6) Error (or deviation) from the infinite plate case for water supersaturation

Normally only the temperature, ice supersaturation and water supersaturation fields are saved for output. An example of the computed temperature and water supersaturation fields is shown in Figure 17.

4.2 Model Describing Shear Flow and Transient Supersaturation

The second numerical model developed computes the steady state conditions in a vertical plane parallel to the flow direction with considerations given to the shear flow profile, the temperature and total pressure dependencies of the vapor and thermal diffusivities. Previous computations by other investigators have dealt with slab flow with constant values for the coefficients (Saxena et al., 1970; Fitzgerald, 1970; Brown et al., 1979; Fukuta and Saxena, 1979a).

The shear flow velocity profile between parallel plates is given by

$$V(z) = - \frac{1}{2\mu} \frac{dP_a}{dy} z(H-z) \ , \qquad (1)$$

where μ is the viscosity of the fluid, $\frac{dP_a}{dy}$ the total pressure gradient in the direction of the flow and H the distance between the plates (Clark and Kays, 1953; Schlichting, 1955; Bird, 1960: White, 1974). The z direction is taken in the vertical between the plates and y in the direction of the flow. This profile is referred to as Poiseuille flow and has a non-slip condition at the boundaries and a maximum velocity midway between the plates.

The equations used for heat and vapor transport, respectively, are

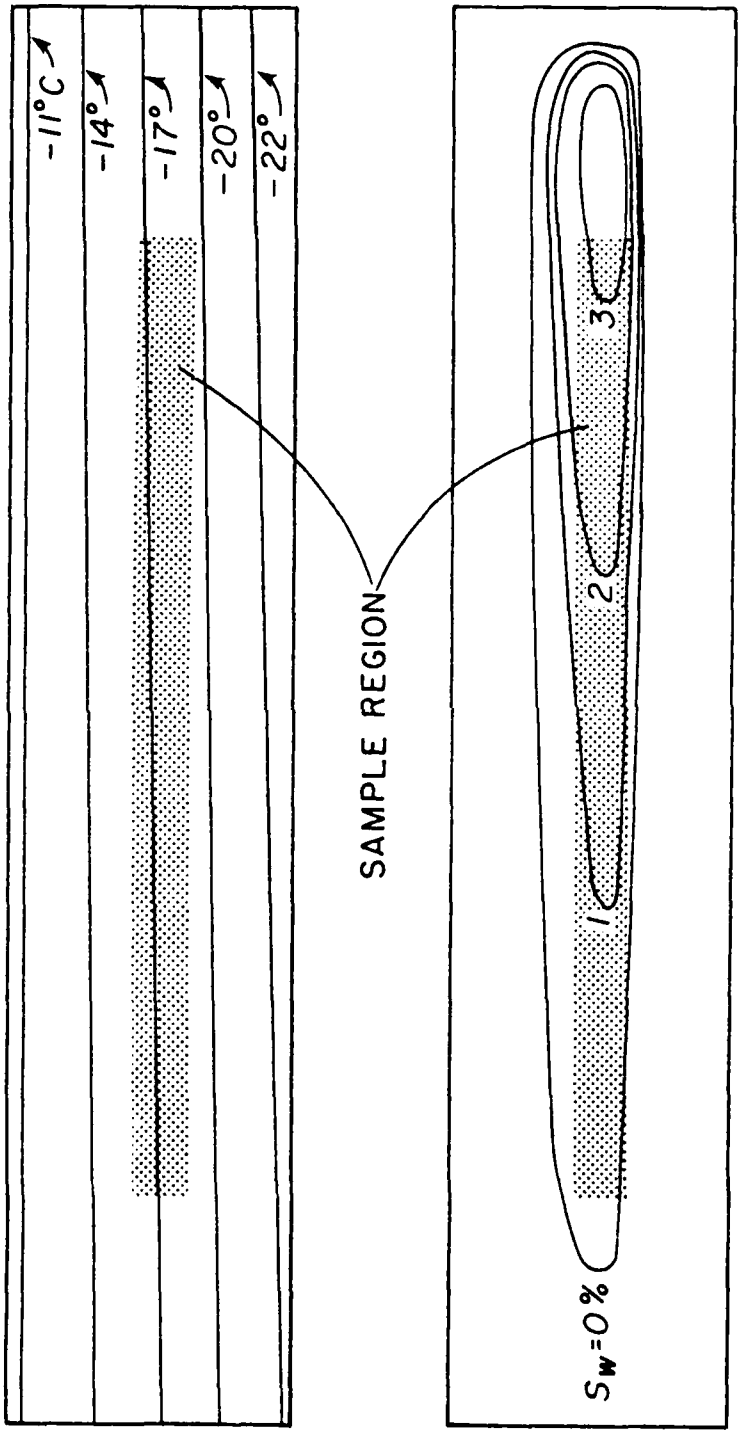

Figure 17. An example of the computed temperature and water supersaturation fields in the plane perpendicular to the flow.

$$\frac{\partial T}{\partial t} = \underbrace{\kappa\nabla^2 T + \nabla\kappa\nabla T}_{a} - V\frac{\partial T}{\partial y} \qquad (2)$$

$$\frac{\partial P}{\partial t} = \underbrace{D\nabla^2 P + \nabla D\nabla P}_{b} - V\frac{\partial P}{\partial y} \quad , \qquad (3)$$

where κ and D are the thermal and vapor diffusivities, respectively (Jakob and Hawkins, 1957; Kays, 1966; Kutateladze, 1966; Gebhart, 1971). Scale analysis indicate that the horizontal components of the terms in (a) of Eq. (2) and (b) of Eq. (3) are negligible when compared to the vertical components. Therefore, Eqs. (2) and (3) reduce to

$$\frac{\partial T}{\partial t} = \kappa\frac{\partial^2 T}{\partial z^2} + \frac{\partial \kappa}{\partial z}\cdot\frac{\partial T}{\partial z} - V\frac{\partial T}{\partial y} \text{ , and} \qquad (4)$$

$$\frac{\partial P}{\partial t} = D\frac{\partial^2 P}{\partial z^2} + \frac{\partial D}{\partial z}\cdot\frac{\partial P}{\partial z} - V\frac{\partial P}{\partial y} \quad . \qquad (5)$$

The resulting equations are second order non-linear partial differential equations. Since what is needed is the steady state profiles for the interior of the chamber excluding the initial time dependent parts, setting $\partial T/\partial t = 0$ in Eq. (4) and $\partial P/\partial t = 0$ in Eq. (5) gives the steady state profiles. Equations (4) and (5) were integrated numerically under the measured boundary conditions of the experiments. The numerical schemes used are presented in Appendix B. The integration schemes are stable and converge nicely. The minimum simulated time used was that required for the slowest parcel to be advected through the chamber. This turned out to be always longer than the time required to reach steady state if the chamber had been static.

The primary uses for this model are to determine exactly what the

transient conditions are and where steady state is reached in each section of the chamber. Furthermore, the model was used to determine to what temperature the recycled filtered air needed to be warmed in order to avoid condensation in the prechamber as shown in Figure 7 of Chapter 3. The model was also used to determine how long the vapor delay at the beginning of the postchamber need be to avoid transient supersaturations. The model also verifies that ice supersaturation is maintained throughout the postchamber, so that no crystals are lost by sublimation.

This model was not run for each experiment because it takes approximately 4.5 hours on the Terak. It was, however, run for representative temperatures and flow speeds used in the studies. Figure 18 shows a plot of the temperature, ice supersaturation, and water supersaturation for the sample region of a typical experiment. It is interesting to note the behavior of the supersaturation curves at the beginning of the postchamber. This definitely shows that transient supersaturations are avoided.

The present model has produced some results which are somewhat different from previous computations. Substitution of the shear flow profile for the slab flow results in steady state being attained approximately 15% sooner but made no change in the steady state values. This is not surprising since as steady state is achieved when $\frac{\partial T}{\partial y}$ and $\frac{\partial P}{\partial y}$ go to zero, and Eqs. (2) and (3) reduce to the slab flow case.

The addition of total pressure and temperature dependencies on the thermal and vapor diffusivities (Boynton and Brattzin, 1929; List, 1966) also produced some changes in both the transient time and the steady state values. The total pressure lowering results in a significant

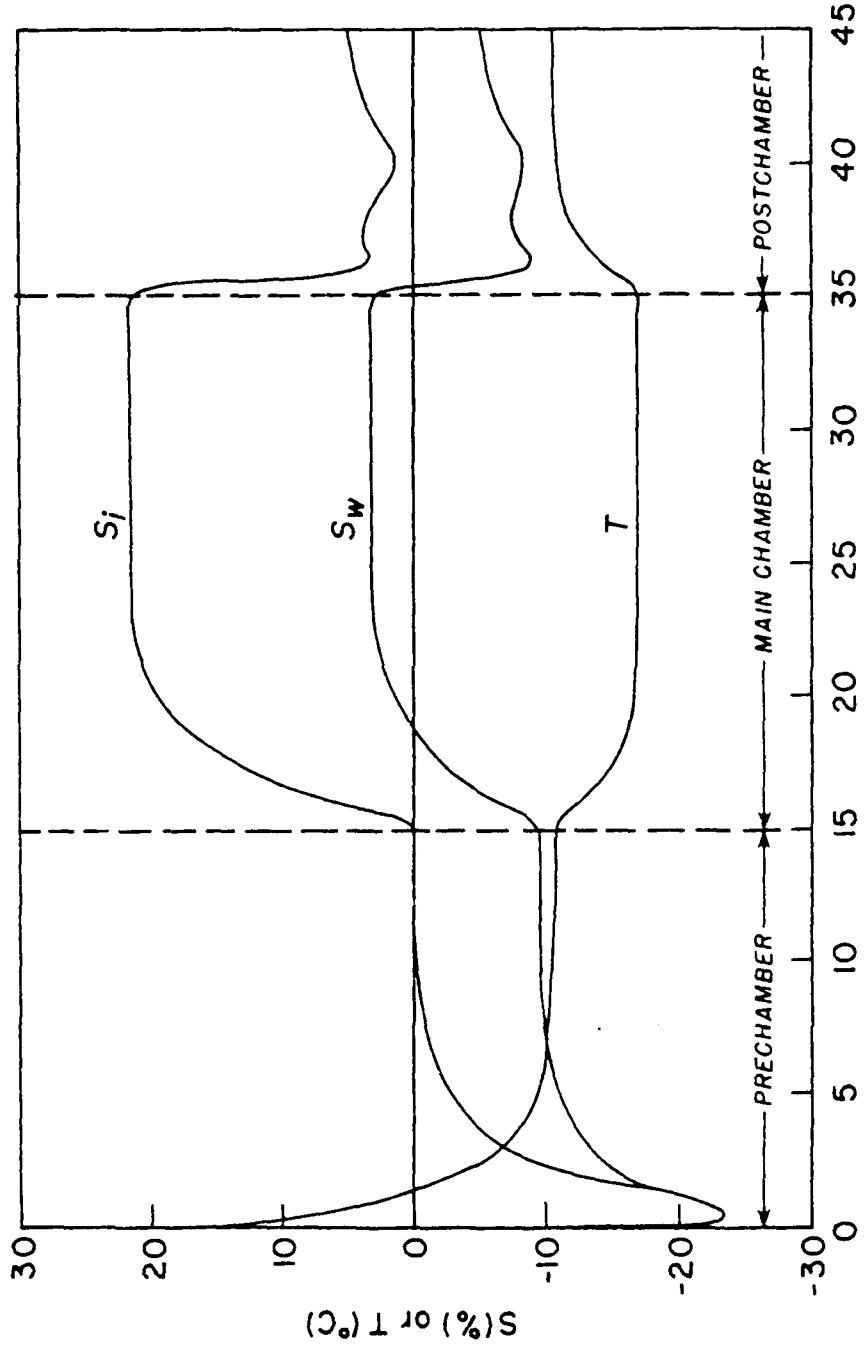

Figure 18. The steady state temperature and supersaturation with respect to ice and water for the sample region through the chamber. The top plate temperature is -10°C and the bottom plate -24°C.

reduction in the time required to attain steady state conditions as shown in Figure 19 but has no significant effect on the steady state values themselves. This dependency should certainly be included for laboratories which operate at atmospheric pressures lower than the standard 1000 millibars as well as for any airborne measurements.

The effects of the temperature dependency on the coefficients were found to be a function of the temperature difference between the plates. For thermal diffusion chambers which maintain only small temperature difference, as is the case for those used in CCN studies, the omission of the temperature dependence is not significant. For larger temperature differences, the effect becomes more apparent by making the temperature and vapor pressure profiles slightly non-linear. This factor was not considered by Katz and Mirabel (1975) in their studies which demonstrated the linearity of these profiles. However, since both profiles are affected in the same direction, there is no significant difference in the computed supersaturation fields from those using linear temperature and vapor pressure profiles. This effect in the present study lowers the temperature in the sample layer by 0.2°C from the linear temperature profile but produces no appreciable change in the supersaturation fields.

4.3 Experimental Verification of the Numerical Models

There are several experimental checks which can be done to verify the numerical models. First, since the volume flow rate is measured, using the chamber dimensions and the shear flow velocity profile, the maximum velocity can be computed. Using smoke in the sample layer and positioning it midway between the plates, the flow speed is measured

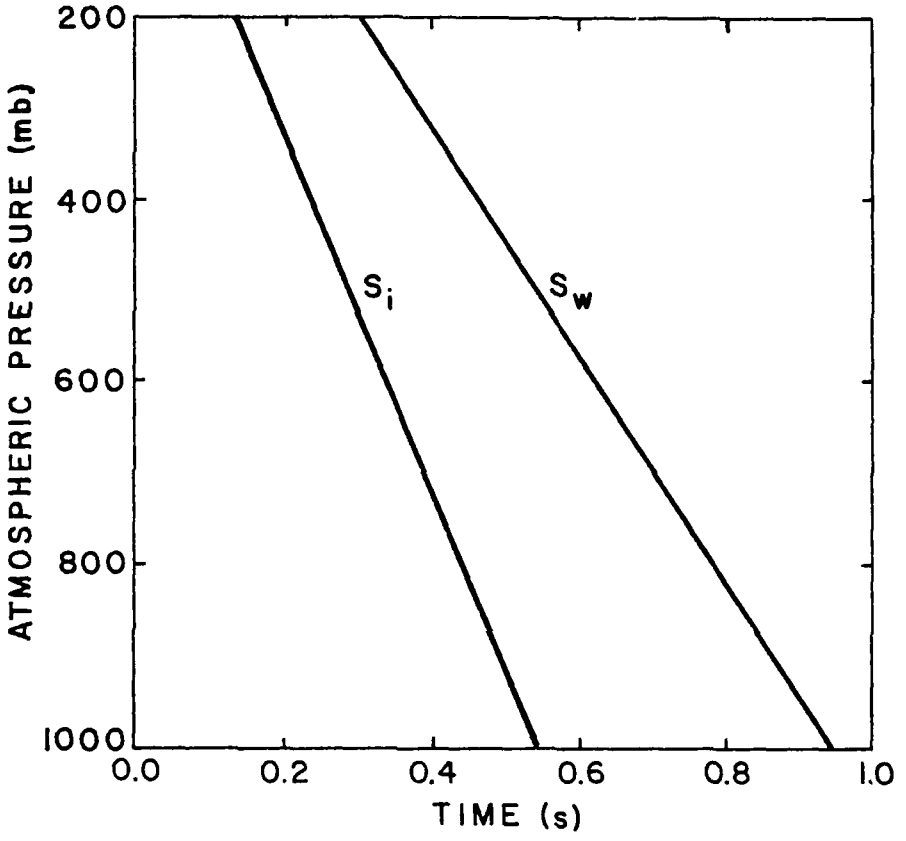

Figure 19. The time required for the sample to reach within 10% of the steady state values in the main chamber as a function of the total atmospheric pressure. S_i and S_w are the supersaturations with respect to ice and with respect to water, respectively.

and compared with that computed. A 5 mw helium-neon laser is used for illumination of the smoke. Table 2 shows the results of such a comparison for the maximum velocity through the main chamber. The results are within limits of experimental errors.

Since the CCN in the atmosphere are normally activated at slightly above water saturation (Amelin, 1967), cloud droplet should form in the chamber where the conditions are attained. Each of the models can be verified using this method by illuminating the interior of the chamber with the laser beam and noting the threshold for fog formation. This threshold has been referred to as the fog front (Schaller and Fukuta, 1979). The first model can be verified by determining the position of the fog front across the flow. The second model can be verified by illuminating the chamber along the direction of the flow in a region where water supersaturation exists and determining the distance from the beginning of the chamber to serve within 1.0 cm of the steady state position indicated by the first model and within 2.0 cm of the transient position indicated in the second model. Some experiments produced "droplets" below water saturation. These "droplets" are believed to be haze particles instead of water droplets on the nucleated CCN.

TABLE 2

COMPARISON OF THE COMPUTED AND MEASURED MAXIMUM FLOW VELOCITY IN THE MAIN CHAMBER

Computed Velocity	Measured Velocity	Relative Error
4.2 cm s^{-1}	4.4 cm s^{-1}	5%
5.5	5.6	2
6.9	6.5	6
8.6	8.3	4
11.2	10.3	9
13.2	12.5	6

CHAPTER 5

SAMPLING PROCEDURE

5.1 Preparation of the Chamber

The preparation of the chamber for operation requires approximately 1.5 hours when starting from room temperature. The procedure is simple and does not require the full time attention of the operator. Distilled water is used for the ice surfaces to insure high accuracy values for the boundary vapor pressures. Most of these procedures were discussed in the previous chapter but will be briefly repeated here to clarify the sequence of events in the chamber preparation.

The tape is applied to the outside edges of the top plate and the predetermined amount of water is poured on the bottom plates where ice surfaces are required. The 1 cm wide copper plate is placed at the beginning of the postchamber. The circulating refrigerated bath thermostat is set at the desired top plate temperature and the bath is started. When the top plate temperature reaches -5°C, the ice layer is applied and the tape removed. Cooling of the bottom plate of the main chamber is begun with the thermoelectric modules on the cold side drawing 8 amperes (the maximum rating of the modules) and those on the warm side, 5 amperes (the maximum ouput of the power supply). After the water in the main chamber freezes, the plastic sheet to control dentrite growth is inserted. The chamber is closed, and the top plate sealed with the water bead, thermal insulation installed over the top of the chamber. After the bottom plate of the main chamber reaches the

desired level, the thermoelectric modules or the heating wire on the warm side of the bottom plate are adjusted to achieve the final steady state temperature profile across the plate. The thermoelectric modules on the cold side continue to draw 8 amperes of electric current, i.e. continue at the maximum output. The plastic sheet is removed just prior to the beginning of sampling.

5.2 Sampling Procedures

The collection film is placed in the postchamber and 3 to 6 minutes are allowed for the temperature to stabilize. During this time, the water droplets condense on the film with the slightly warmer top plate being the vapor source. For warm temperatures (top plate less than -10°C), the film is pretreated in the freezer. The air outlet device is attached to the postchamber and sampling is begun by adjusting the total flow rate to the desired level and then adjusting the sample flow rate as required. The automatic temperature recording is started when the flow begins. An identification number and the date are recorded with the temperature. The sampling continues until the desired sample air volume is processed in the chamber. The sample flow is terminated but the filtered air flow continues for 15 seconds to guarantee all the sample air has exited the chamber. The temperature recording is terminated when the flow is stopped.

5.3 Ice Crystal Counting

After the sampling is completed, the cold cover with the ice coated inner surface is placed over the ice collection film and both are moved together to the freezer. The film is placed on a metal plate maintained around -10°C and illuminated for photographing. For crystals too small to

photograph, the wetted cover of 1 cm height is placed over the film until the crystals grow to adequate size. Ice crystals on the film are photographed with the identification number. All the films are photographed from the same angle using the same illumination source. After photographing, the film is removed from the freezer and dried at room temperature for reuse.

Three by five inch prints are made for each sampling case and overlayed with a grid showing the regions or lanes of constant supersaturation and temperature. The total number of crystals in each lane is counted and recorded. An average temperature is computed for each of the nine temperature locations for use in the numerical models.

5.4 Sample Smoke Generation and Collection

The artificial ice nuclei used for the experiments were generated in the laboratory. The particle number conentration was determined by the ultramicroscope method (Green and Lane, 1964). It is important to determine the particle sizes and concentration (Gerber, et al,; 1970). The particle size was estimated by measuring the particle fall velocity and determining the particle size using the Stokes fall velocity equation with the Cunningham correction (Fuchs, 1964). After the number concentration was determined, an appropriate amount was transferred to a large box (approximately 1.5 m^3) to furnish a sample source with a reasonable concentration and large enough not to be significantly affected by the removal of sample for a measurement. Silver iodide smoke was generated by placing the powder on a 25 cm length of 32 gauge platinum wire and heating the wire. The platinum wire requires 42 watts for smoke generation, attaining a temperature of approximately

1000°C. A photograph of the AgI smoke generation is presented in Fig. 20(a).

DN smoke was produced using the device shown in Fig. 20(b). The copper tube wound around the soldering iron is heated and then DN powder is forced through the coil using the syringe. The powder vaporizes as it moves through the heated coil and the smoke forms as the vapor exits and mixes with outside air. The smoke is then collected for use.

The average diameter of the AgI particles was 0.05 μm and that of DN 0.1 μm. The size distribution are shown in Fig. 21. The values for DN are from Vasquez (1980).

Natural nuclei were collected from air sampled from the 8th floor of the Browning Building, northeast corner, University of Utah. The sample was brought into the laboratory through flexible steel plastic coated conduit. The kaolinite sample was produced by grinding the kaolinite into a fine powder and shaking it inside a 10 liter plastic jug. Sampling was begun after a 10 minute delay to allow large particles to settle.

Figure 20(a). Photograph of the platinum wire assembly used in the generation of silver iodide.

Figure 20(b). Photograph of the device used in the generation of the DN smoke.

(a)

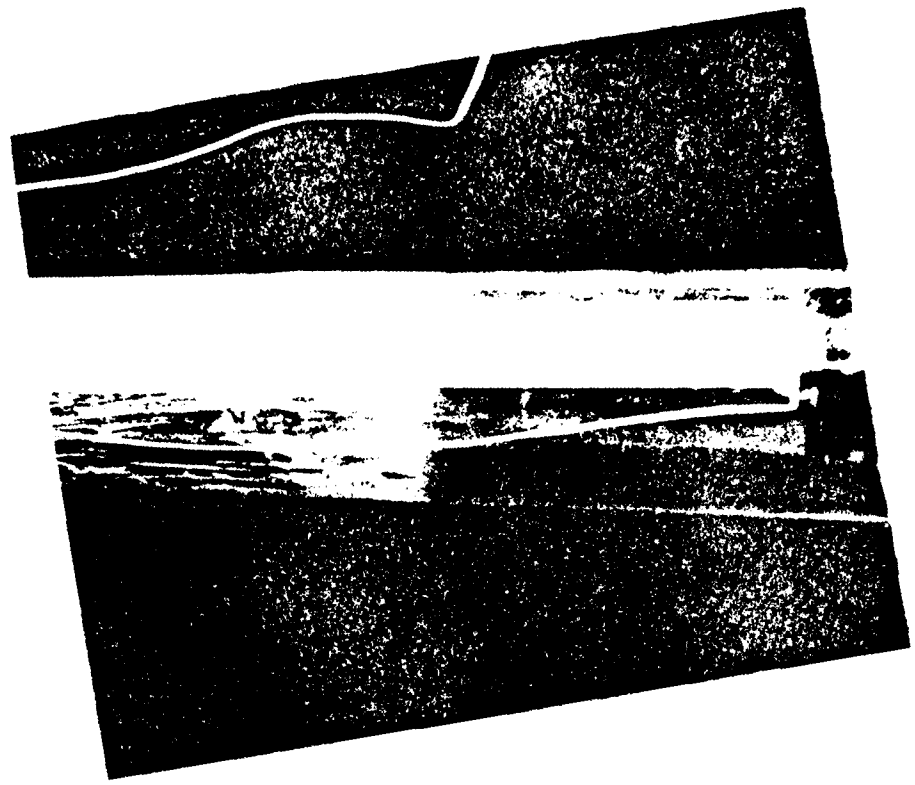

(b)

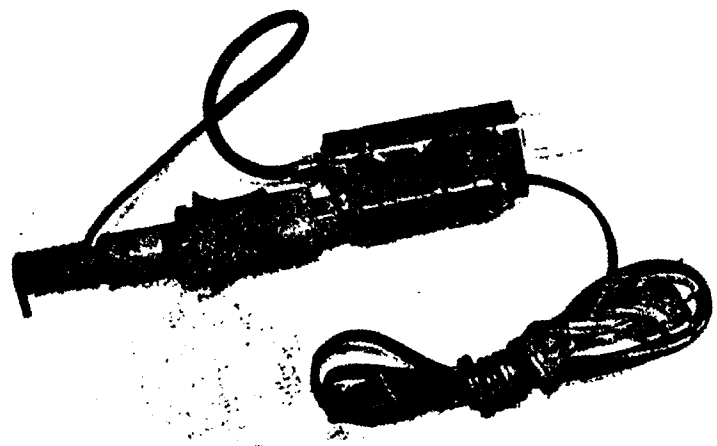

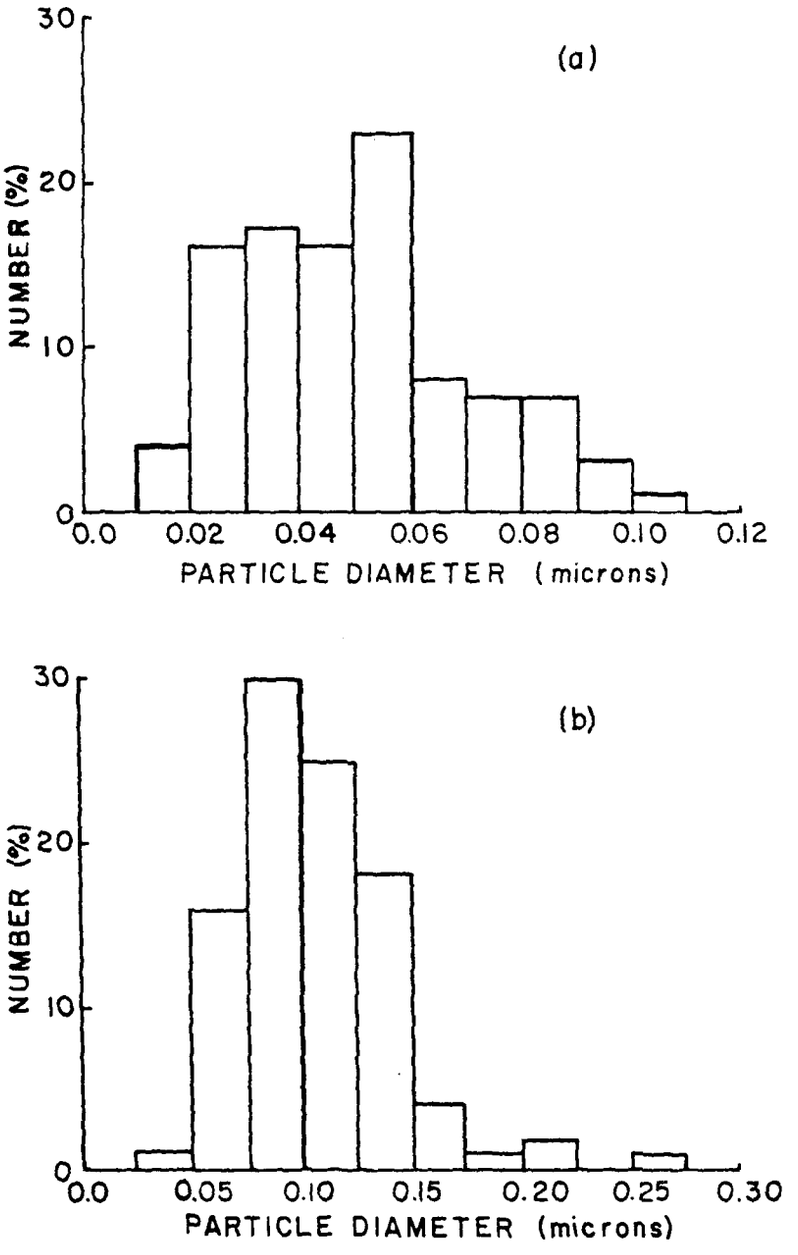

Figure 21. Size distributions for AgI (a) and DN (b).

CHAPTER 6

EXPERIMENTAL RESULTS

6.1 Silver Iodide (AgI)

Silver iodide was selected for study since it has been the most commonly used artificial ice nuclei (Flecher, 1962; Mossop, 1968, Cooper, 1970; Mason, 1971; Dyer, 1978). Figure 22 shows the results of experiments under different temperatures and ranges of supersaturation. Below water saturation, nucleation of water condensation does not take place. Therefore, ice nucleation that occurs under this condition must belong to the deposition nucleation mechanism. Since there is little change in the activation mode of the ice nuclei across water saturation up to at least one percent water supersaturation, it appears that condensation-freezing is not occurring until water supersaturation conditions of at least this value are reached.

Ice nucleation is a time dependent phenomenon (Warburton and Heffernan, 1964; Anderson and Hallett, 1976) and it is important to verify that the present method of ice nucleus activation and counting indeed detects all the active nuclei under the chosen condition. For the condensation-freezing mechanism studied in these experiments, varying the flow speed through the chamber can provide the data needed for this verification. If all the time dependent nucleus activations are completed within a period of time shorter than available in the main chamber, the total number of ice crystals will remain the same regardless of the flow rate within a reasonable limit. Three

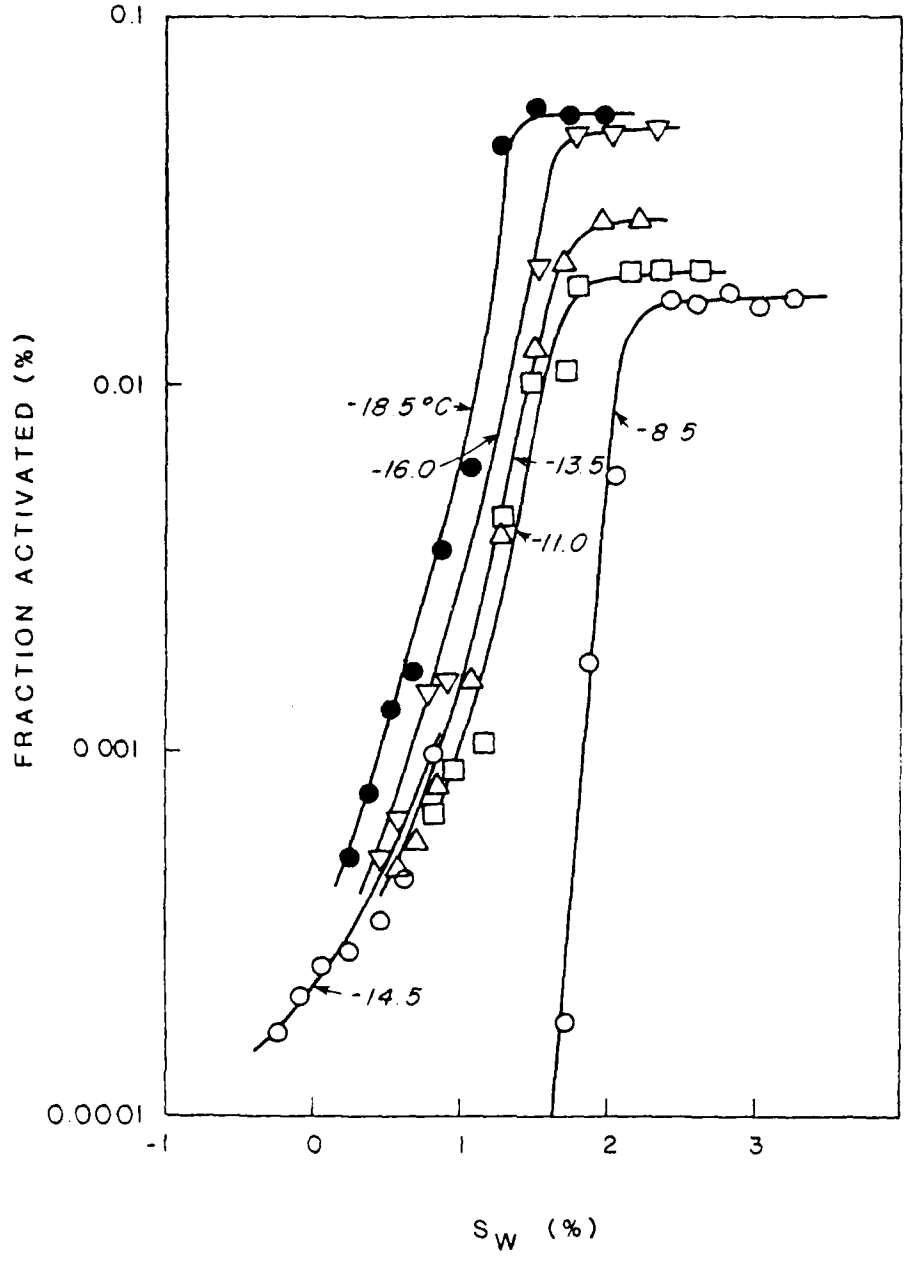

Figure 22. Active number of AgI particles as a function of supersaturation with respect to water at different temperatures.

AD-A092 479 AIR FORCE INST OF TECH WRIGHT-PATTERSON AFB OH F/G 4/2
A NEW HORIZONTAL GRADIENT, CONTINUOUS FLOW, ICE THERMAL DIFFUSI--ETC(U)
JUN 80 E M TOMLINSON
UNCLASSIFIED AFIT-CI-80-210 NL

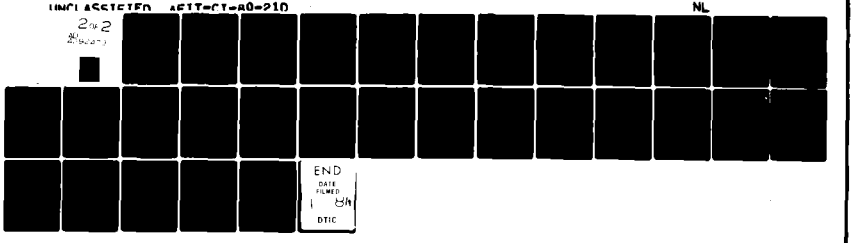

experiments were performed with the same sample source (AgI) under identical chamber conditions except for varying flow speeds. The results are presented in Fig. 23. The average diameter of the smoke particles is 0.05 μm. For the case where most of the crystals were collected on the film, a near normal distribution was observed. The other cases show the same shape with different half widths. If these distributions are taken to be normal and the curves extrapolated beyond the limits of the collection film, then the areas under the curves are found to agree within 10%. This indicates that the total number of crystals nucleated remain the same for all three cases, i.e. there is no dependence of the total number of ice nucleations on sample flow speed within the limits of these experiments. It should be observed that the number density of collected crystals falls to zero for the two slower flow speeds before the end of the collection film. Thus, it was confirmed that the necessary period of time for all the nucleation to take place is shorter than that available in the main chamber. For deposition regions of these experiments, similar results were noted although the number of crystals was much smaller.

The experimental results shown in Fig. 22 clearly indicate that the threshold for condensation-freezing is highly temperature dependent for a given supersaturation value. The maximum number of nuclei activated is also shown to depend on the temperature. For a given temperature this maximum is reached at some water supersaturation value but becomes independent of it thereafter. It should be noted that even for the coldest temperature, this maximum is not reached until around 1.5 percent water supersaturation and requires 2.5 percent at -8.5°C. These high supersaturation values are rarely found in nature. Hence,

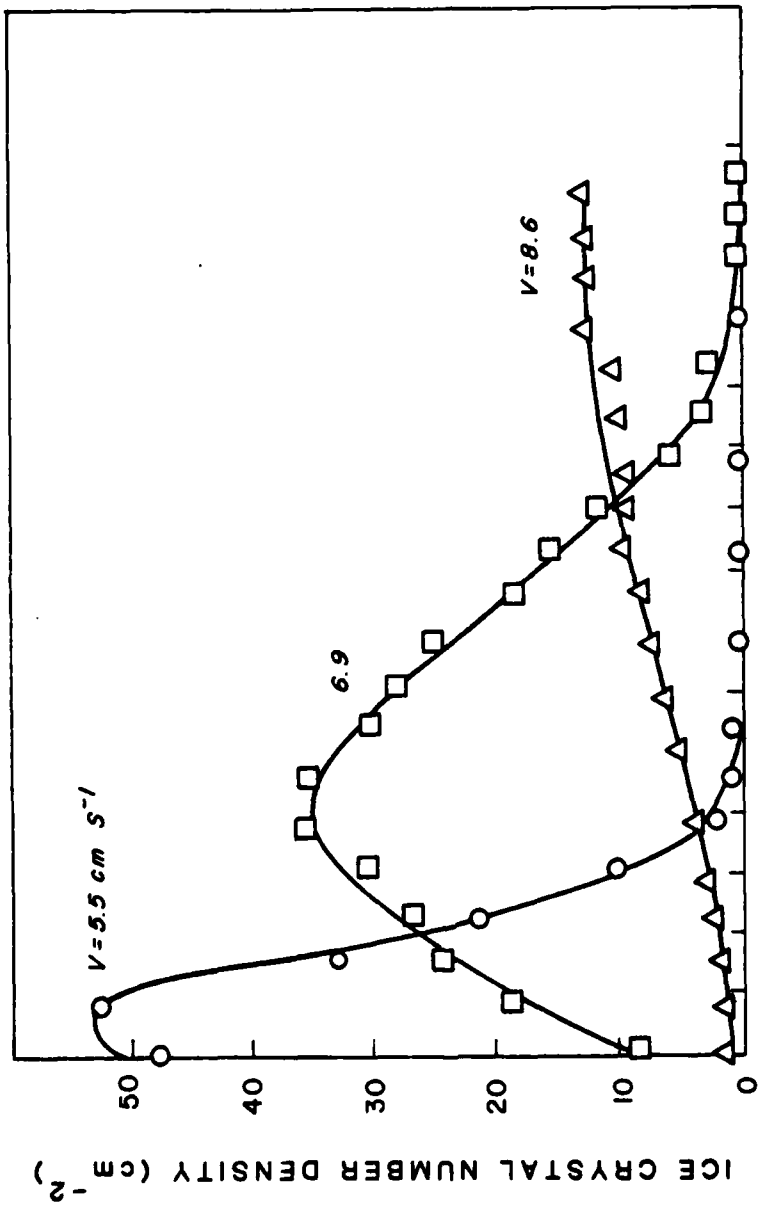

Figure 23. Distribution of the ice crystal number density on the collection film for different sample flow speeds. The sample is AgI, the temperature is -9.9°C and the water supersaturation is 2.6%. The distance is measured from the leading edge of the collection film.

it is clear from these data that cloud chambers which permit unrealistically high supersaturations to occur do not give a true indication of the activation characteristics of these nuclei in real clouds but instead are probably yielding the maximum values indicated in Figure 22.

Only a very small fraction of the particles are activated below 1.0 percent water supersaturation at any of the temperatures studied suggesting that the condensation-freezing mechanism is not yet present. Previous studies by other investigators (Isono, 1966; Schaller and Fukuta, 1979) have shown that the condensation-freezing threshold is lower than that given here, the difference being attributed to the wide difference in instrument accuracy. In addition, a very low number of nuclei are activated below water saturation in the deposition nucleation region. Measurements were also done with the AgI smoke generated in air filtered of CCN and IN. Additionally, samples were used from a ground AgI generator furnished by North American Weather Consultants of Salt Lake City. No significant change from the above results were observed with either sample.

6.2 1,5 - Dihydroxynaphthalene (DN)

Experiments similar to those for AgI were performed using 1,5 - dihydroxynaphthalene (DN). The results are shown in Figure 24. The average size of the smoke particles is 0.1 μm. The results are similar to those for AgI but differ in the following respects. The water supersaturation threshold required for condensation-freezing nucleation is lower, suggesting that it is more effective in natural cloud environments. Again as was the case for AgI, a maximum value for the active number of nuclei is evident at high supersaturations. However,

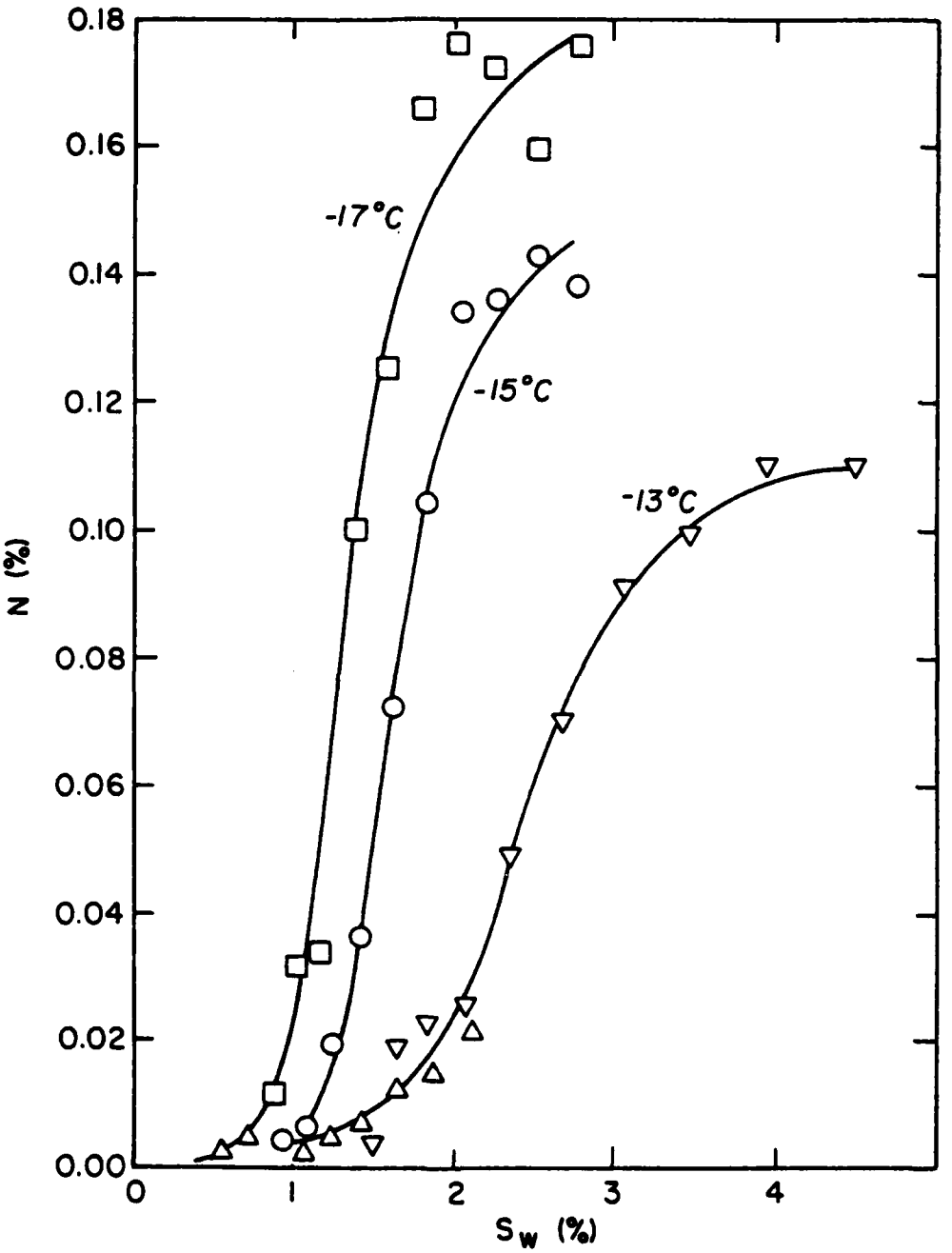

Figure 24. Active number of DN particles as a function of supersaturation with respect to water at different temperatures.

the total number of particles which are active is greater by a factor of about three. For the warmer temperatures in Figure 24 the rate at which the number of active DN particles changes with increased supersaturation is slower than for AgI showing that once the condensation-freezing supersaturation threshold is exceeded, AgI reaches its maximum active number more rapidly than does DN although DN achieves a higher activation number.

6.3 Natural Nuclei

Using this instrument, natural nuclei have been studied under accurately controlled temperature and supersaturation without substrate effects. The results are shown in Figure 25. It can be seen in the figure that the data are considerably scattered as would be expected from the variation of natural aerosol particle conditions. There appears to be little or no supersaturation dependency for values of water supersaturation between -1.0 and 1.0 percent for temperature ranges from -17° to -22°C. However, for increases in water supersaturation beyond 1.0 percent, there is indeed an overall increase in the number of active nuclei. An order of magnitude increase occurs in the number as the value of water supersaturation changes from 1.0 to 2.5 percent.

There were several occasions where an interesting phenomenon was observed. On March 26, 1980, measurements were performed with outdoor air at the northeast corner of the 8th floor of the Browning Building, University of Utah. The chamber temperature was -23°C with water supersaturations ranging from 2.9 to 4.0 percent, the conditions where active nuclei are normally observed. However, only three nuclei were

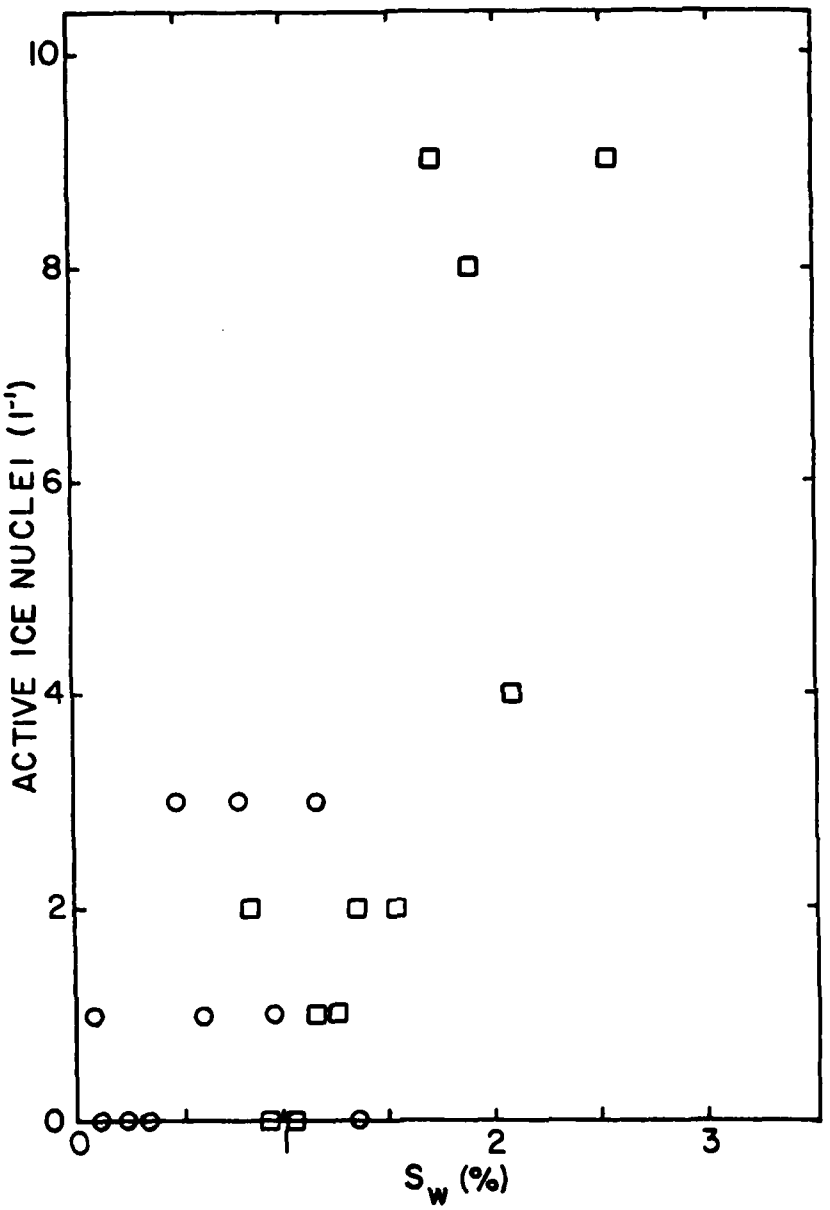

Figure 25. Active number of natural nuclei as a function of supersaturation with respect to water. The temperature is -22°C.

activated in 10 liters of sample air. It was later confirmed that snow was falling at the time of the sampling indicating that either the ice nuclei in the environment had previously been activated and the resulting crystals excluded out of the sample air or were scavenged from the air by the falling snowflakes.

Another interesting observation occurred on March 4, 1980. Outdoor air was being sampled at -20°C with water supersaturation ranging from 1.0 to 3.1 percent. A measurement just prior to a snowshower resulted in about 10 active nuclei per liter in a 10 liter air sample. The next sampling, taken during the snowshower, showed a drop to less than one nucleus per liter, i.e. only four nuclei were activated in the 10 liter sample air. Since loading and evaporation of hydrometeors are the main reasons for downdraft development, it is possible that downdraft air contains ice nuclei from evaporated ice crystals. A downdraft prior to the approaching snowshower may have brought down active nuclei which were once involved in hydrometeor formation process. This sequence clearly demonstrates the high variability of natural ice nuclei in both time and space.

6.4 Kaolinite

Since kaolinite has been studied by other investigators (Roberts and Hallett, 1967; Schaller and Fukuta, 1979) and has shown some ability to act as an ice nuclei, several measurements were performed using it. The results are presented in Figure 26. Although considerable spread is seen in the data, the same basic insensitivity to water supersaturation is evident as observed with natural nuclei until high water supersaturations are reached.

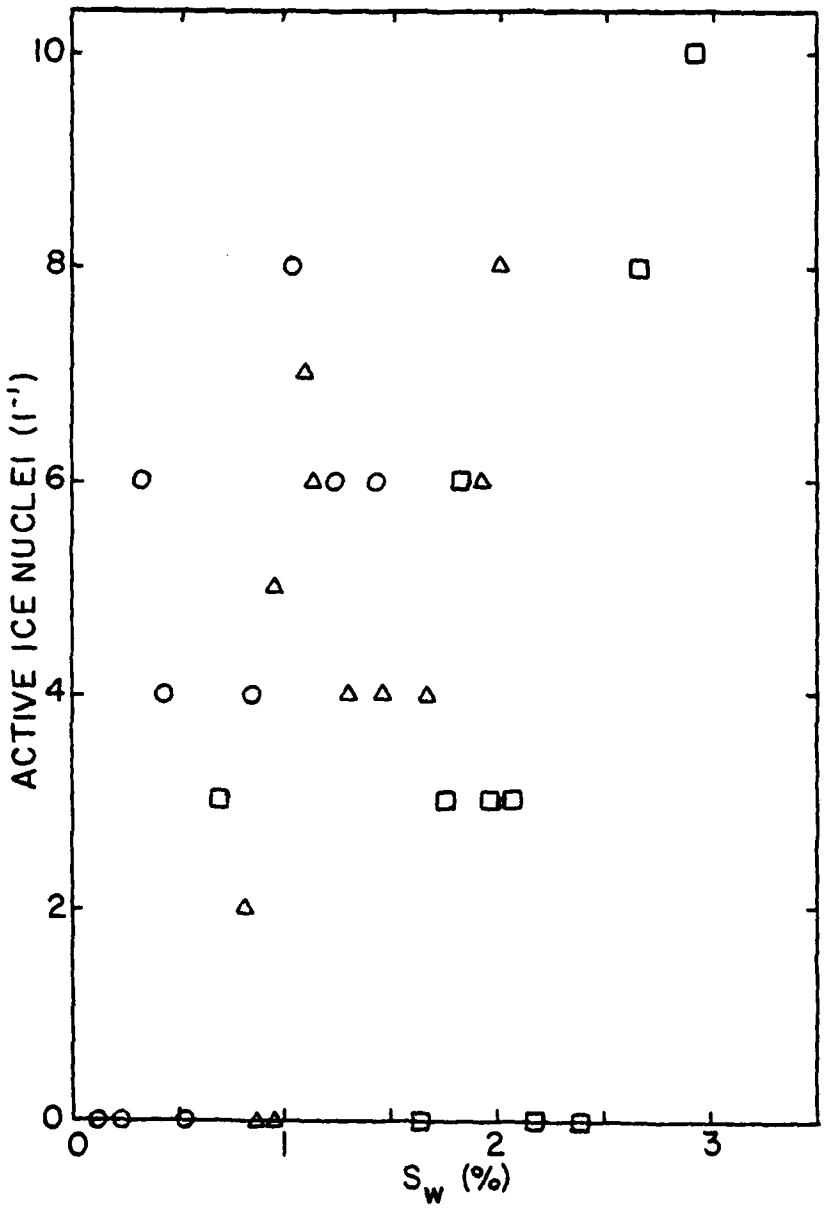

Figure 26. Active number of active kaolinite particles as a function of supersaturation with respect to water. The temperature is -22°C.

CHAPTER 7

CONCLUSIONS

In the attempt to develope a new horizontal gradient, continuous flow, ice thermal diffusion chamber, a number of new schemes have been devised. The subsequent use of the chamber for ice nucleus measurements has resulted in a number of new findings both in the technology of instrumentation for ice nucleus studies and in the mechanisms and nucleating behaviors of both natural and artificial ice nuclei. The main contributions are listed below.

7.1 Instrument Development

The possibility for a high accuracy continuous flow, horizontal gradient, ice thermal diffusion chamber was suggested by Fukuta and Saxena (1979a). Development of the instrument presented in this study is a demonstration of the concept. Main features of the developed instrument are as follows:

1. The continuous flow, horizontal gradient, ice thermal diffusion chamber has been constructed and successfully tested. It consists of three sections which preprocess the sample, activate the nuclei under clearly defined conditions and collect the nucleated crystals for counting. In the chamber, the sample air is continuously processed under a range of supersaturations at approximately constant temperature.

2. A scheme of sandwiching the sample air between layers of filtered air and of positioning the sample air in a region of clearly defined temperature and supersaturation has been used. By controlling the temperature and vapor pressure of the filtered air before entering the chamber, transient condensation in the sample is avoided during preprocessing.
3. Heat pipes have been effectively utilized for temperature uniformity in the direction of the flow in the main chamber.
4. For the region where the cold sample air enters the warmer postchamber after processing, a unique vapor diffusion delay scheme is applied to avoid transient supersaturations.
5. An ice coating technique is developed to produce smooth ice layers of uniform thickness on the inner surfaces of the top and bottom plates.
6. A new ice crystal collection scheme is used which integrates the ice crystals activated under the same conditions. Uncertainties associated with the optical methods used in other diffusion chambers are eliminated.
7. Use of filtered air to separate the sample from the walls eliminates any wall effect on the sample. Moreover, it keeps the sample air away from the convectively unstable region adjacent to the walls.
8. The flow control scheme employed permits accurate monitoring and control while introducing the sample without any contamination from pumps or flowmeters.
9. The condensation-freezing and deposition mechanisms of ice nucleation have been effectively isolated while the contact

freezing mechanism has been excluded. This feature permits the identification of the mechanism involved in ice nuclei activation.

10. A scheme for high accuracy computerized real-time temperature measurement has been developed. This permits precise determination of the interior temperature and supersaturation fields.
11. Complete numerical models have been constructed which furnish detailed temperature and vapor pressure fields. The models not only compute steady state values but verify that transient supersaturations and wall effects are avoided.

7.2 New Findings with Ice Nuclei Measurements

The accurate temperature and supersaturation control available with the present instrument has enabled the findings of new as well as more detailed behaviors of both artificial and natural ice nuclei. The main findings are listed below.

1. The rate of deposition nucleation is much lower than that of condensation-freezing for all nuclei in all temperature ranges studied.
2. For AgI of average particle size 0.05 μm, only a very small fraction (less than 0.001%) are found to be active below 1.0 percent water supersaturation and for DN of average particle size 0.1 μm, a higher number (as high as 0.02%) are active.
3. For temperatures warmer than -10°C, the condensation-freezing mechanism is not effective for AgI. This finding can have a significant implication on the use of AgI in weather modification.

4. The total number of active ice nuclei at high supersaturations is about three times larger for DN than that for AgI.
5. Once the condensation-freezing thresholds are reached for AgI and DN, further increases in supersaturation makes AgI to reach its maximum active number more quickly than DN.
6. Natural and kaolinite nuclei show little supersaturation dependency below 1.0 percent water supersaturation.
7. Natural and kaolinite nuclei show an increase in activity by an order of magnitude as the water supersaturation increases from 1.0 to 2.5 percent. Instruments which allow such high supersaturation values to occur will therefore yield high active nuclei counts and the results should be considered unreliable.
8. For natural nuclei, large variances were observed with high counts in cloud downdrafts and low counts during precipitation.

7.3 Possible Future Applications of the New Chamber

The new features of the present chamber, i.e. the accurate and simultaneous display of a range of supersaturation with continuous sampling, suggest application of the chamber in a number of areas.

1. The present chamber may be used as a standard for detecting condensation-freezing and deposition nucleations and other chambers and methods of ice nucleus detection may be calibrated against it.
2. Further detailed studies of condensation-freezing and deposition nucleations may be carried out for different chemicals, particles of different sizes, effects of additives on ice

nucleus smoke and nucleation time lag.

3. The present chamber may be used to obtain real time data of natural nuclei.
4. Contact freezing mechanism may be isolated out of mixed nucleation processes using the present chamber.

APPENDIX A

NUMERICAL MODEL TO DETERMINE WALL EFFECTS AND THE STEADY STATE SUPERSATURATION FIELDS

This numerical model computes the steady state temperature and vapor pressure values inside a rectangular thermal diffusion chamber using the same approach presented by Tomlinson and Fukuta (1979). The model provides for temperature and vapor pressure gradients and therefore the supersaturation profile inside the chamber utilizing thermal gradients on both the top and bottom plates although in this study, only the bottom plate maintains a gradient. This generality allows the model to be used for other thermal diffusion chambers. Also, the model is not limited to subfreezing temperatures and can be used for any CCN spectrometer of rectangular geometry such as that of Fukuta and Saxena (1979a and b).

The model assumes linear temperature gradients in the vertical direction on the side walls and throughout the chamber interior as justified by Tomlinson and Fukuta (1979). On the other hand, any temperature profile can be imposed on the top and bottom plates. In this study, the top plate is kept isothermal. The temperature is recorded during the experiments at three locations across the bottom plate of the main chamber. The temperature profile for the bottom plate is taken to be a quadratic function of the distance horizontally across the flow direction which satisfies these three temperature points. Vapor pressure is assumed to be ice saturated on all the boundaries

(water saturation for temperatures above 0°C) and is computed using a sixth degree polynominal (Rasmussen, 1978).

The equations used are taken from Carslaw and Jaeger (1957). In order to use these equations, the boundaries have to be expressed by a sine series. A sufficient number of terms are used to express exact values at the boundary grid points. The following series were used:

$$P_B(x) = \sum_{n=0}^{\infty} a_n \sin \frac{n\pi x}{A} ,$$

$$P_L(x) = \sum_{n=0}^{\infty} b_n \sin \frac{n\pi z}{B} , \text{ and}$$

$$P_R(z) = \sum_{n=0}^{\infty} c_n \sin \frac{n\pi z}{B} ,$$

where a_n, b_n, and c_n are the amplitudes of wave number n in each series (Spiegel, 1968). The lower left corner of the chamber is the origin for the coordinate system as shown in Figure A1. The x direction is horizontal and has a maximum at z = A on the right boundary. The z direction is vertical and has a maximum at z = B on the top boundary.

As discussed in Chapter 4, the vapor pressure can be expressed by the following sum as shown in Figure A2:

$$P(x,z) = P_1 + P_2(x,z) + P_3(x,z) + P_4(x,z) + P_5(x,z)$$

The equations used to compute each pressure component are as follows:

$$P_1 = P_{BL},$$

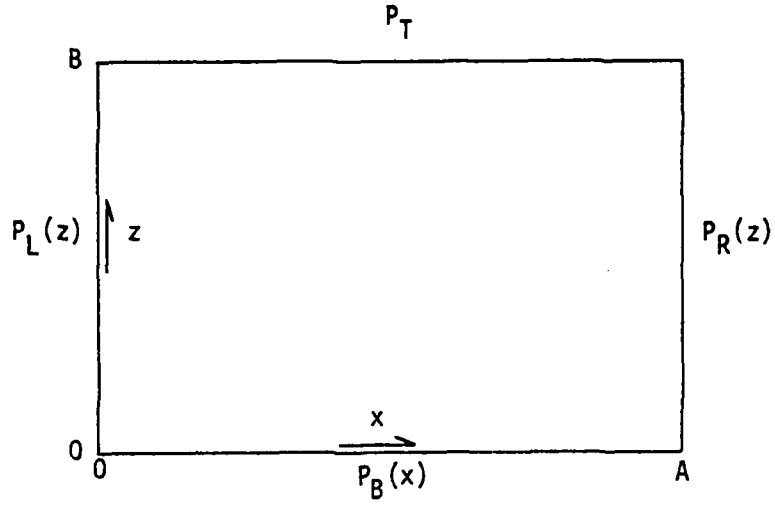

Figure A1. The coordinate system used in the model and the boundary vapor pressures.

$$P_2 = \frac{4\Delta P}{\pi} \sum_{n=0}^{\infty} \frac{1}{(2n+1)} \sin \frac{(2n+1)\pi x}{a} \sinh \frac{y(2n-1)\pi}{a} \operatorname{cosech} \frac{(2n+1)b\pi}{a},$$

$$P_3 = \sum_{n=0}^{\infty} a_n \sin \frac{n\pi x}{A} \sinh \frac{(B-y)n\pi}{A} \operatorname{cosech} \frac{nB\pi}{A}$$

$$P_4 = \sum_{n=0}^{\infty} b_n \sin \frac{n\pi y}{B} \sinh \frac{xn\pi}{B} \operatorname{cosech} \frac{nA\pi}{B}$$

$$P_5 = \sum_{n=0}^{\infty} c_n \sin \frac{n\pi y}{B} \sinh \frac{(A-x)n\pi}{B} \operatorname{cosech} \frac{nA\pi}{B}$$

The values can be computed on any grid desired. The grid used in this study was 16 X 11 which gives a 1 cm resolution horizontally and 0.06 cm vertically for the chamber dimensions. After the temperature and vapor pressure fields are computed, supersaturation values with respect to both water and ice are determined (water only for temperatures above 0°C). These values are compared with the supersaturation values for the same boundary conditions in the infinitely wide parallel plate case and the error fields are estimated accordingly. It is these error fields which are used to determine the extent of the wall effects. The supersaturation values for the interior of the chamber are used in the studies.

The error associated with the wall effect is presented in Figure A2. Several cases were computed for various chamber heights. It should be noted that the wall effect increases significantly as the chamber height increases.

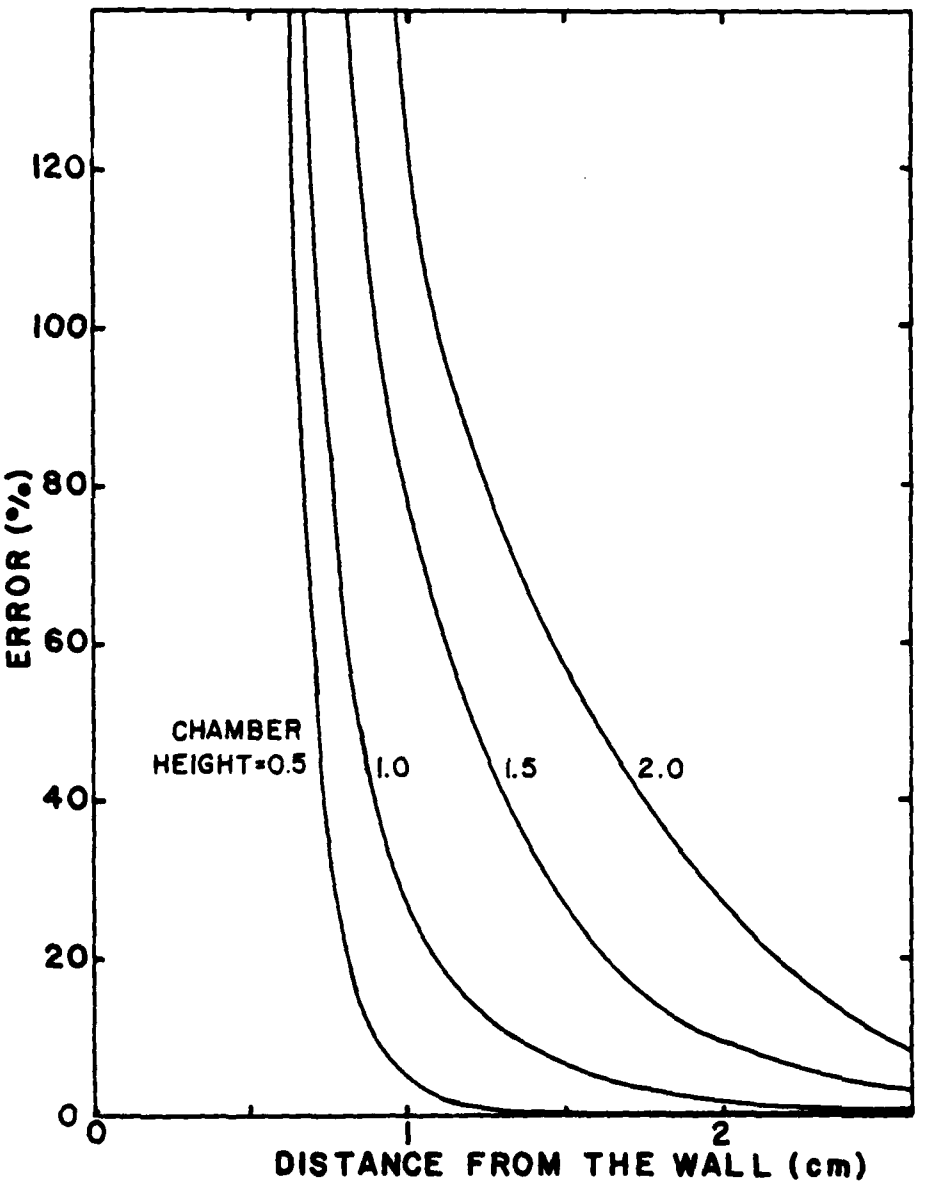

Figure A2. Error in the water supersaturation field due to the wall effect for a rectangular ice thermal diffusion chamber. Various heights in centimeters are plotted.

APPENDIX B

SCHEMES USED IN THE NUMERICAL INTEGRATION

As presented in Chapter 4, the equations describing the temperature and vapor pressure profiles between the plates of the thermal diffusion chamber with flow are

$$\frac{\partial T}{\partial t} = \kappa \frac{\partial^2 T}{\partial z^2} + \frac{\partial \kappa}{\partial z} \cdot \frac{\partial T}{\partial z} - V(z) \frac{\partial T}{\partial y} \tag{B1}$$

$$\frac{\partial P}{\partial t} = D \frac{\partial^2 P}{\partial z^2} + \frac{\partial D}{\partial z} \cdot \frac{\partial P}{\partial z} - V(z) \frac{\partial P}{\partial y} \tag{B2}$$

The velocity profile for shear flow between parallel plates is

$$V(z) = - \frac{1}{2\pi} \frac{\partial P}{\partial y} z (H-z)$$

Here V(z) is a known function of z for any given pressure $\frac{\partial P}{\partial y}$. Both κ and D are functions of total pressure and temperature (List, 1966). For a given altitude, i.e. atmospheric pressure, κ and D become functions of temperature only. Hence, for every time step κ and D are determined at each interior grid point after the temperature at that grid point is computed.

The time derivatives $\frac{\partial T}{\partial t}$ and $\frac{\partial P}{\partial t}$ are approximated with the second order centered approximations as follows:

$$\frac{\partial T}{\partial t} \doteq \kappa \frac{T_{j,k}^{n+1} - T_{j,k}^{n-1}}{2\Delta t} \tag{B3}$$

$$\frac{\partial P}{\partial t} \simeq D \frac{p^{n+1}_{j,k} - p^{n-1}_{j,k}}{2\Delta t} \tag{B4}$$

where n is the index for time, j the index for the y direction, k the index for the z direction, and Δt the time increment. The second derivatives are approximated by the second order scheme as follows:

$$\kappa \frac{\partial^2 T}{\partial z^2} \simeq \kappa \frac{T^{n-1}_{j+1,k} + T^{n-1}_{j-1,k} - 2T^{n-1}_{j,k}}{(\Delta z)^2} \tag{B5}$$

$$D \frac{\partial^2 P}{\partial z^2} \simeq D \frac{p^{n-1}_{j+1,k} + p^{n-1}_{j-1,k} - 2p^{n-1}_{j,k}}{(\Delta z)^2} \tag{B6}$$

where Δz is the vertical grid spacing. The first derivatives in space are approximated using second order centered differencing except for the right (downstream) boundary. The scheme is as follow:

$$V(z) \frac{\partial T}{\partial y} \simeq V(z) \frac{T^{n}_{j+1,k} - T^{n}_{j-1,k}}{2\Delta y} \tag{B7}$$

$$V(z) \frac{\partial P}{\partial y} \simeq V(z) \frac{p^{n}_{j+1,k} - p^{n}_{j-1,k}}{2\Delta y} \tag{B8}$$

$$\frac{\partial \kappa}{\partial z} \simeq \frac{\kappa^{n}_{j,k+1} - \kappa^{n}_{j,k-1}}{2\Delta z} \tag{B9}$$

$$\frac{\partial D}{\partial z} \simeq \frac{D^{n}_{j,k+1} - D^{n}_{j,k-1}}{2\Delta z} \tag{B10}$$

where Δy is the horizontal grid spacing along the direction of the flow. On the right boundary, the following upstream scheme is used:

$$V(z) \frac{\partial T}{\partial y} \simeq V(z) \frac{T^{n}_{j,k} - T^{n}_{j-1,k}}{\Delta y} \tag{B11}$$

$$V(z)\frac{\partial T}{\partial y} \doteq V(z)\frac{p^n_{j,k} - p^n_{j-1,k}}{\Delta y} \qquad (B12)$$

For the beginning of the postchamber where the vapor pressure is delayed, the new lower boundary condition produced some oscillations in the solution field. The use of the upstream differencing scheme in the advection term resulted in a stable solution field. Since this is only a first order scheme, the horizontal grid spacing is reduced by a factor of ten in order to maintain the overall accuracy.

The vertical grid spacing is z = 0.06 cm and the horizontal grid spacing is y = 0.5 cm except as mentioned above at the beginning of the postchamber where it is decreased to 0.05 cm. These grid spacings proved adequate to resolve the conditions inside the chamber. This was verified by decreasing the grid spacing by a factor of two and noting no change in the solution field. The time increment was selected to satisfy the following stability requirements:

$$\frac{\text{maximum } |V|\Delta t}{\Delta y} < O(1) \qquad (B13)$$

$$\frac{\text{maximum } (\kappa, D)\Delta t}{\Delta z^2} < O(1) \qquad (B14)$$

$$\frac{\text{maximum } (\frac{\partial \kappa}{\partial z}, \frac{\partial D}{\partial z})\Delta t}{\Delta z} < O(1) \qquad (B15)$$

Although each of these critria is sufficient only in particular more idealized equations, satisfaction of the most stringent of (B13, B14, B15) produced stable solutions.

REFERENCES

Alofs, D. J., and J. C. Carstens, 1976: Numerical simulation of a widely used cloud nucleus counter. J. Appl. Meteor., 15, 350-353.

Amelin, A. G., 1967: Theory of Fog Condensation. Israel Program for Scientific Translations, Jerusalem, p. 24.

Anderson, B. J., and J. Hallett, 1976: Supersaturation and time dependence of ice nucleation from the vapor on single crystal substrates. J. Atmos. Sci., 33, 822-832.

Bergeron, T., 1935: On the physics of clouds and precipitation. "Proc. 5th Assembly U.G.G.I.", Lisbon, 2, 156.

Bigg, E. K., 1957: A new technique for counting ice-forming nuclei in aerosols. Tellus, 9, 394-400.

_____, G. T. Miles, and K. J. Heffernan, 1961: Stratospheric ice nuclei, J. Met., 18, 804.

_____, S. C. Mossop, R. T. Meade and N. S. C. Thorndike, 1963: The measurement of ice nuclei concentrations by means of millipore filters. J. Appl. Meteor., 2, 266-269.

Bird, R. B., W. E. Stewart and E. N. Lightfoot, 1960: Transport Phenomena. Wiley, 780 pp.

Boynton, W. P., and W. H. Brattain, 1929: Interdiffusion of gases and vapors. International Critical Tables of Numerical Data, Physics, Chemistry, and Technology, Vol. 5, p62.

Brown, J. T., Jr., and F. D. Schowengerdt, 1979: Analysis of a continuous flow parallel plate thermal diffusion cloud chamber. J. Aerosol Sci., 10, 339-348.

Carslaw, H. S., and J. C. Jaeger, 1955: Conduction of Heat in Solids. Oxford Univ. Press, 217-221.

Clark, S. H., and W. M. Kays, 1953: Laminar-flow forced convection in rectangular tubes. Trans. ASME, 75, 859-866.

Cooper, C. F., and W. C. Jolly, 1970: Ecological effects of silver iodide and other weather modification agents. A review. Water Resources Res., 6, 88-79.

Dunn, P., and D. A. Reay, 1978: Heat Pipes. Pergamon Press, New York, pp 299.

Dyer, R. M., and B. A. Kumkel, 1978: "A comparison of the theoretical and experimental results in supercooled stratus dispersal." AFGL-TR-0193, Air Force Surveys in Geophysics, 395.

Elliott, W. P., 1971: Dimensions of thermal diffusion chambers. J. Atmos. Sci., 28, 810-811.

Fitzgerald, J. W., 1970: Non-steady-state supersaturations in thermal diffusion chambers. J. Atmos. Sci., 27, 70-72.

_____, 1972: On the computation of steady-state supersaturations in thermal diffusion chambers. J. Atmos. Sci., 29, 779-781.

Fletcher, N. H., 1958: Size effect in heterogeneous nucleation. J. Chem. Phys., 29, 572-576, 31, 1136.

Fuchs, N. A., 1964: The Mechanics of Aerosols. Pergamon Press, 408 pp.

Fukuta, N., 1966: Activation of atmospheric particles as ice nuclei in cold and dry air. J. Atmos. Sci., 23, 741-750.

_____, and V. K. Saxena, 1979a: The principle of a new horizontal thermal gradient cloud condensation nucleus spectrometer. J. Rech. Atmos., 13, 169-188.

_____, and V. K. Saxena, 1979b: A horizontal thermal gradient cloud condensation nucleus spectrometer. J. Appl. Meteor., 18, 1352-1362.

Gagin, A., and B. Terliuc, 1968: A modified Wieland-Twomey, thermal-diffusion cloud nuclei counter. J. Rech. Atmos., 3, 73-77.

Gebhart, B., 1971: Heat transfer, McGraw-Hill, 596 pp.

Gerber, H., P. A. Allee, U. Katz, C. I. Davis and L. O. Grant, 1970: Some size distribution measurements of AgI nuclei with an aerosol spectrometer. J. Atmos. Sci., 27, 1060-1067.

_____, 1976: Activity and size of aggregate thermal AgI particles. "The Third International Workshop on Ice Nucleus Measurements," Laramie, Wy., 75-90.

Goroch, A., and J. Carstens, 1972: An analysis of wall effects in the modified Wieland-Twomey, thermal-diffusion cloud nuclei counter of Gagin and Terliuc. J. Rech. Atmos., 6, 669-672.

UNCLASS

SECURITY CLASSIFICATION OF THIS PAGE (When Data Entered)

REPORT DOCUMENTATION PAGE

READ INSTRUCTIONS BEFORE COMPLETING FORM

1. REPORT NUMBER: 80-21D
2. GOVT ACCESSION NO: AD-A092 479
3. RECIPIENT'S CATALOG NUMBER:

4. TITLE (and Subtitle): A New Horizontal Gradient, Continuous Flow, Ice Thermal Diffusion Chamber and Detailed Observation of Condensation-Freezing and Deposition Nucleations

5. TYPE OF REPORT & PERIOD COVERED: MS/PhD/DISSERTATION

6. PERFORMING ORG. REPORT NUMBER:

7. AUTHOR(s): Edward Mason Tomlinson

8. CONTRACT OR GRANT NUMBER(s):

9. PERFORMING ORGANIZATION NAME AND ADDRESS: AFIT STUDENT AT: University of Utah

10. PROGRAM ELEMENT, PROJECT, TASK AREA & WORK UNIT NUMBERS:

11. CONTROLLING OFFICE NAME AND ADDRESS: AFIT/NR, WPAFB OH 45433

12. REPORT DATE: June 1980

13. NUMBER OF PAGES: 109

14. MONITORING AGENCY NAME & ADDRESS (if different from Controlling Office):

15. SECURITY CLASS. (of this report): UNCLASS

15a. DECLASSIFICATION DOWNGRADING SCHEDULE:

16. DISTRIBUTION STATEMENT (of this Report)

APPROVED FOR PUBLIC RELEASE; DISTRIBUTION UNLIMITED

17. DISTRIBUTION STATEMENT (of the abstract entered in Block 20, if different from Report)

18. SUPPLEMENTARY NOTES

APPROVED FOR PUBLIC RELEASE: IAW AFR 190-17

Air Force Institute of Technology (ATC)
Wright-Patterson AFB, OH 45433

Fredric C. Lynch

FREDRIC C. LYNCH, Major, USAF
Director of Public Affairs

19. KEY WORDS (Continue on reverse side if necessary and identify by block number)

20. ABSTRACT (Continue on reverse side if necessary and identify by block number)

ATTACHED

8011 24 153

DD FORM 1 JAN 73 1473 EDITION OF 1 NOV 65 IS OBSOLETE

UNCLASS

SECURITY CLASSIFICATION OF THIS PAGE (When Data Entered)

ABSTRACT

It is well recognized that conditions in the environment surrounding ice nucleu (IN) particles must be accurately controlled in order to understand their nucleation behavior. Concerning the condensation-freezing and deposition mechanisms of ice nucleation, the main factors representing the environment are supersaturation and supercooling (temperature). Starting from the concept of the wedge-shaped ice thermal diffusion chamber of Schaller and Fukuta, and that of the Fukuta-Saxena cloud condensation nucleus (CCN) spectrometer, and by additionally considering operational efficiency and accuracy, a continuous-flow, horizontal gradient, ice thermal diffusion chamber has been developed. The chamber consists of three parts, i.e., preprocessing, main activation and ice crystal settling sections. A common top plate is used for all three sections and is held isothermal using a circulating bath while a temperature gradient is maintained across the bottom plate of the main section by applying thermoelectric modules. In the preprocessing and main sections, both plates are covered with ice. A newly developed method is applied to smoothly coat ice on the plates. This configuration of the main section results in a nearly constant temperature horizontally in the direction across the sample flow, and produces a range of supersaturations. Heat pipes are utilized on the sides of the bottom plate to insure temperature uniformity along the direction of the flow. The sample volume is sandwiched in the region of maximum supersaturation between layers of filtered and predried air such that,

as the sample enters the main section, a nearly constant supersaturation is achieved vertically through the sample without transient supersaturations. The preprocessing section is held isothermal at the top plate temperature. The design and flow of the main section permit the nucleated ice crystals to be carried into the ice crystal settling section without loss. The bottom plate in the settling section is maintained at a temperature slightly lower than that of the top plate. Formation of transient supersaturations at the entrance of the settling section has been avoided by delaying vapor diffusion while allowing thermal diffusion to proceed. The problem of transient supersaturation development has been examined for shear (Poiseuille) flow cases using a numerical method instead of the commonly used slab flow assumption. Wall effects have also been computed for the supersaturation distribution. The stability of the sample flow throughout the entire chamber has been confirmed with smoke tests. A new method for ice crystal detection has been developed and is employed in the ice crystal settling section. Mylar copy film (carbon paper) holding condensed water droplets is placed in the settling section. Ice crystals nucleated in the main section fall on the film and grow to visible sizes in the presence of the droplets. The positions of the ice crystals across the flow direction give the supersaturations and temperatures at which they nucleated. The optimum design of the chamber in terms of the height, width, length and flow speed has been determined.

Two numerical models have been developed to compute the temperature and supersaturation fields within the chamber. The first computes the steady state conditions in a vertical plane perpendicular to the flow

and includes the wall effects. The second computes the steady state conditions in a vertical plane parallel to the flow using the shear flow velocity profile and the total pressure- and temperature-dependent coefficients for vapor and thermal diffusion.

The increased accuracy of the developed chamber has resulted in several significant new findings. For all the temperature and supersaturation ranges studied, the rate of deposition nucleation is much lower than that for condensation-freezing. For silver iodide (AgI) particles of average diameter 0.05 μm, only a small fraction are active below 1% water supersaturation, while for 1,5 - dihydroxynaphthalene (DN) of average diameter 0.1 μm, a much larger fraction are active. The total number of active nuclei for these samples was approximately three times greater for DN than for AgI at high supersaturations. For temperatures warmer than -10°C, the condensation-freezing mechanism is not effective for AgI. Natural nuclei and kaolinite show little supersaturation dependence below 1% water supersaturation and as much as an order of magnitude increase as water supersaturation increases from 1% to 2.5%. Additionally for natural nuclei, large variances were observed with high counts in cloud downdrafts and low counts during precipitation.

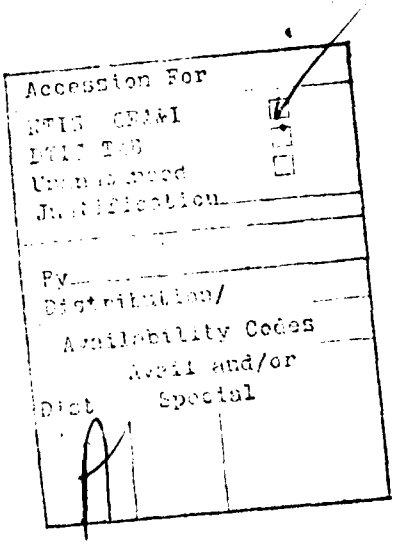

Green, H. L. and W. R. Lane, 1964: Particulate Clouds: Dust, Smokes, and Mists. E. & F. N. Spon. Ltd., Universities Press, Belfast, Ireland, 241-244.

Hallett, J., 1971: Address. "The Second International Workshop on Condensation and Ice Nuclei." Fort Collins, Co., p10.

Heist, R. H., and H. Reiss, 1973: Investigation of the homogeneous nucleation of water vapor using a diffusion cloud chamber. J. Chem. Phys., 59, 665-671.

Hudson, J. G., and P. Squires, 1973: Evolution of a recording continuous cloud nucleus counter. J. Appl. Meteor., 12, 175-183.

_____ and P. Squires, 1976: An improved continuous flow cloud chamber. J. Appl. Meteor., 15, 776-782.

Isono, K., and Ishizaka, Y., 1972: An experimental study on ice nucleating properties of alpha-, beta-, and gamma-silver iodide. J. Rech. Atmos., 6, 283-300.

Jakob, M., and G. A. Hawkins, 1957: Elements of Heat Transfer. Wiley, 3rd Ed., New York, pp. 169.

Katz, J. L., and B. J. Ostermier, 1967: Diffusion cloud-chamber investigation of homogeneous nucleation. J. Chem. Phys., 47, 478-487.

_____ and P. Mirabel, 1975: Calculation of supersaturation profiles in thermal diffusion chambers. J. Atmos. Sci., 32, 646-652.

Kays, W. M., 1966: Convection Heat and Mass Transfer. McGraw-Hill, New York, 387pp.

Kline, D. B., and G. W. Brier, 1961: Some experiments on measurements of natural nuclei. Mon. Wea. Rev., 89, 263-272.

Kutateladze, S. S. and V. M. Borishanskii, 1966: A Concise Encyclopedia of Heat Transfer. Pergamon Press, New York, 489pp.

Langer, G., 1971: NCAR modification of Bigg-Warner expansion chamber counter. "The Second International Workshop on Condensation and Ice Nuclei." Fort Collins, Co., 67-68.

_____, 1973: Analysis of results from Second International Ice Nuclei Workshop with emphasis on expansion chambers, NCAR counters, and membrane filters. J. Appl. Meteor., 12, 991-999.

Langsdorf, A., Jr., 1936: A continuously sensitive cloud chamber. Phys. Rev., 49, 422.

List, R. J., 1966: Smithsonian Meteorological Tables, 6th Rev. Ed., Smithsonian Institute Press, 527 pp.

Mason, B. J., 1971: The Physics of Clouds. Clarendon Press, Oxford, 481 pp.

_____ and J. Hallett, 1956: Artificial ice-forming nuclei. Nature, 177, 681-683.

Mossop, S. C., 1968: Silver iodide as nucleus for water condensation and crystallization. J. Rech. Atmos., 3, 185-190.

Ohtake, T., 1976: Settling cloud chamber for ice nucleus counting. "The Third International Workshop on Ice Nucleus Measurements", Laramie, Wy., 151-158.

Petterssen, S., 1958: Introduction to Meteorology. McGraw-Hill, New York, 327 pp.

Podzimek, J., 1971: Address. "The Second International Workshop on Condensation and Ice Nuclei", Fort Collins, Co., 3-5.

Radke, L. F., and P. V. Hobbs, 1969: An automatic cloud condensation nuclei counter. J. Appl. Meteor., 8, 105-109.

Rasmussen, L. A., 1978: On the approximation of saturation vapor pressure. J. Appl. Meteor., 17, 1564-1565.

Rodgers, R. R., 1976: A Short Course in Cloud Physics. Pergamon Press, Oxford, 227 pp.

Roberts, P., and J. Hallett, 1967: A laboratory study of the ice nucleation properties of some mineral particulates. Quart. J. Roy. Meteor. Soc., 94, 25-34.

Rosen, J. M., and D. J. Hofmann, 1977: Balloonborne measurements of condensation nuclei. J. Appl. Meteor., 16, 56-62.

Saxena, V. K., J. N. Burford, and J. L. Kassner, Jr., 1970: Operation of a thermal diffusion chamber for measurements of cloud condensation nuclei. J. Atmos. Sci., 27, 73-80.

Schaefer, V. J., 1946: The production of ice crystals in a cloud of supersaturated droplets. Science, 104, 457-459.

_____, 1952: Continuous cloud chamber for studying small particles in the atmosphere. Ind. Eng. Chem., 44, 1381-1383.

_____, 1954: Ice crystals formed spontaneously by the rapid expansion of moist air. J. Colloid. Sci., 9, 175-181.

_____, 1971: Remarks. "The Second International Workshop on Condensation and Ice Nuclei," Fort Collins, Co., p. 6.

Schaller, R. C. and N. Fukuta, 1971: Ice nucleation by aerosol particles: Experimental studies using a wedge-shaped ice thermal diffusion chamber. J. Atmos. Sci., 36, 1788-1802.

Schlichting, H., 1955: Boundary Layer Theory, Pergamon Press, 647 pp.

Sears, F. W., and M. W. Zemansky, 1962: University Physics, Addison-Wesley Publishing Co., Inc., Reading, Mass., p 909.

Sinclair, D., and G. S. Hoopes, 1975: A continuous flow nucleus counter. Aerosol Sci., 6, 1-7.

Sinnarwalla, A. M., and D. J. Alofs, 1973: A cloud nucleus counter with long available growth time. J. Appl. Meteor., 12, 831-835.

Spiegel- M. R., 1968: Mathematical Handbook, McGraw-Hill Book Co., New York, 271 pp.

Squires, P., 1971: Keynote Address. "The Second International Workshop on Condensation and Ice Nuclei." Fort Collins, Co., p 7.

_____, 1972: Diffusion chamber for the measurement of cloud nuclei. J. Rech. Atmos., 6, 565-571.

Tomlinson, E. M., and N. Fukuta, 1979: Aspect ratio of thermal diffusion chambers. J. Atmos. Sci., 36, 1362-1365.

Twomey, S., 1963: Measurements of natural cloud nuclei. J. Rech. Atmos., 1, 101-105.

Vali, G., 1976: Preface. "The Third International Workshop on Ice Nucleus Measurements." Laramie, Wy., p. 7.

Vasquez, H. R., 1980: Private communication.

Warburton, J. A., and K. J. Heffernan, 1964: Time lag in ice crystal nucleation by silver iodide. J. Atmos. Sci., 3, 788-791

Warner, J., 1957: An instrument for the measurement of freezing nucleus concentration. Bull. Obs. Puy. de Dome, No. 1, 33-46.

Weickmann, H. K., 1971: Address. "The Second International Workshop on Condensation and Ice Nuclei." Fort Collins, Co., p 2.

White, F. M., 1974: Viscious Fluid Flow. McGraw-Hill, New York, 723 pp.

Yang, I. K., 1962: An impaction ice nucleus counter. Bull. Obs. Puy de Dome, No. 3, 112-123.

VITA

Name	Edward Mason Tomlinson
Birthplace	Petersburg, Virginia
Birthdate	11 July, 1944
High School	Powhatan High School Powhatan, Virginia
Universities	University of Richmond Richmond, Virginia 1962-1966 University of Michigan Ann Arbor, Michigan 1967-1968 University of Utah Salt Lake City, Utah 1972-1974
Degrees	Bachelor of Arts in Mathematics, 1966 University of Richmond Master of Science in Meteorology, 1974 University of Utah
Professional and Honorary Organizations	Sigma Xi Pi Mu Epsilon Chi Epsilon Pi Phi Kappa Phi
Publications	"Solution of the Balance Equation Incorporating Fourier Transform and Gauss Elimination," with Jan Paegle. Monthly Weather Review, 103, 528-535. "Fourier Analysis/Gauss Elimination Techniques Applied to the Balance Equation," (Masters Thesis, University of Utah, 1974), 31 pages. "Aspect Ratio of Thermal Diffusion Chambers," with N. Fukuta. Journal of Atmospheric Sciences, 36,1362-1365.